AD-A082 184 BOSTON COLL CHESTNUT HILL MASS DEPT OF PHYSICS F/G 4/1
STUDY OF CHARACTERISTICS OF POLAR CAP AURORAS IN DMSP IMAGES.(U)
FEB 80 M S GUSSENHOVEN AFOSR-79-0012

UNCLASSIFIED AFOSR-TR-80-0214 NL

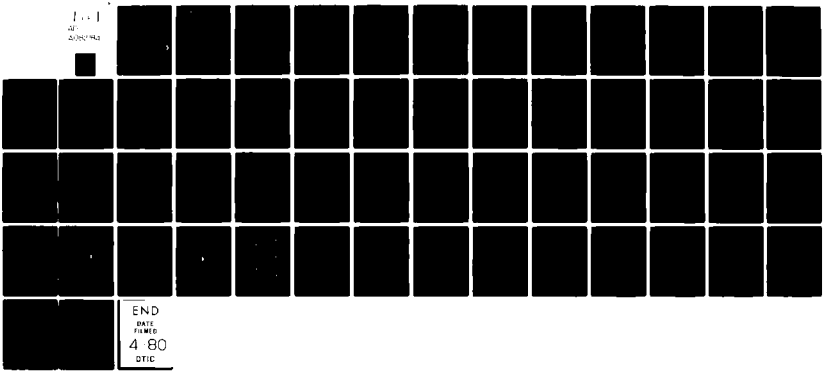

END
DATE FILMED
4 80
DTIC

Study of Characteristics of Polar Cap Auroras in DMSP Images

Final Report
February 29, 1980
AFOSR-79-0012

M. S. Gussenhoven

Physics Department
Boston College
Chestnut Hill, MA 02167

UNCLASSIFIED

SECURITY CLASSIFICATION OF THIS PAGE (When Data Entered)

REPORT DOCUMENTATION PAGE

READ INSTRUCTIONS BEFORE COMPLETING FORM

1. REPORT NUMBER: AFOSR-TR-80-0214	2. GOVT ACCESSION NO.
3. RECIPIENT'S CATALOG NUMBER	
4. TITLE (and Subtitle): Study of Characteristics of Polar Cap Auroras in DMSP Images	5. TYPE OF REPORT & PERIOD COVERED: Final, 1 Oct 78 — 31 Dec., 1979
	6. PERFORMING ORG. REPORT NUMBER
7. AUTHOR(s): M. S. Gussenhoven	8. CONTRACT OR GRANT NUMBER(s): AFOSR-79-0012
9. PERFORMING ORGANIZATION NAME AND ADDRESS: Boston College, Chestnut Hill, MA 02167	10. PROGRAM ELEMENT, PROJECT, TASK AREA & WORK UNIT NUMBERS: 61102F 2311/A1
11. CONTROLLING OFFICE NAME AND ADDRESS: Air Force Office of Scientific Research /NP, Building 410, Bolling AFB, D.C. 20332	12. REPORT DATE: February 29, 1980
	13. NUMBER OF PAGES: 56
14. MONITORING AGENCY NAME & ADDRESS (if different from Controlling Office)	15. SECURITY CLASS. (of this report): Unclassified
	15a. DECLASSIFICATION DOWNGRADING SCHEDULE

16. DISTRIBUTION STATEMENT (of this Report)

Approved for public release - distribution unlimited

17. DISTRIBUTION STATEMENT (of the abstract entered in Block 20, if different from Report)

18. SUPPLEMENTARY NOTES

19. KEY WORDS (Continue on reverse side if necessary and identify by block number)

aurora, electron precipitation, plasma sheet, magnetospheric convection electric field injection boundary, auroral boundary

20. ABSTRACT (Continue on reverse side if necessary and identify by block number)

Energetic electron measurements from a particle detector on the DMSP/F2 satellite have been used to determine the corrected geomagnetic latitude (Λ_{CGM}) of the equatorward boundary of the auroral oval. The satellite was launched into a nearly sun-synchronous, polar orbit centered on the 0700-1900 MLT meridian. Due to the wobble of the dipole and a very slow precessional motion of the orbit more than 6000 boundary crossings could be studied in the 1600-2300 and 0400-1000 MLT sectors. The detectors, which have large geometric

DD FORM 1 JAN 73 1473

Unclassified

factors, look radially away from the earth and detect precipitating electrons with energies between 50eV and 20keV. In the evening sector the equatorward boundaries are precisely determined from the rise in the total electron flux. The morningside boundary cannot always be clearly delineated. Data were divided into one hour magnetic local time bins with ~400 samples per bin. In each of the MLT bins Λ_{CGM} was found to be linearly correlated to the K_p index. Regression values of Λ_{CGM} were projected to the magnetic equatorial plane using the Mead-Fairfield magnetic field model. The projected boundaries are not in good agreement with the injection boundaries of Mauk and McIlwain (1974). They are best fit to boundaries derived using Volland-Stern type electric fields with the axis of symmetry rotated in the evening sector for $K_p < 2$ and into the afternoon sector for $K_p \geq 2$.

INTRODUCTION

The work reported here is a continuation of a larger effort to model particle entry into the extremely high latitude regions of the ionosphere ($\geq 80^{\circ}$CGM). When of sufficient density and energy, electrons precipitating here result in polar cap auroras (more generally referred to as extremely high latitude auroras). A large statistical study using DMSP (Defense Meteorological Satellite Program) optical data (Gussenhoven, 1979) showed that the occurrence of auroras at these latitudes depended primarily on the z-component of the interplanetary magnetic field being positive. They also occurred when magnetic activity, as measured by K_p, was moderate (2-3), while electrojet activity, as measured by A_E, was low. Further, extremely high latitude auroras occur preferentially in local time sectors of the cap according to the y-component of the interplanetary magnetic field, B_y. They have greater frequency of occurrence in the morning for negative B_y, and in the evening for positive B_y. This is in the opposite sense of increases in the polar cap electric field (Heppner, 1972).

Polar cap arcs can be intense and highly structured, but more often they are weak, and difficult to detect in the DMSP images. With the launch of the DMSP-F2 satellite, in September, 1977, which carried two sets of electrostatic analysers (J-sensors) with large geometric factors, (Hardy et al., 1979) electron precipitation in the polar caps could be studied in greater detail. Several characteristics of the electron precipitation were apparent: 1) Morning precipitation patterns differ substantially from evening precipitation patterns. In the morning low energy electrons (< 1keV) precipitate over much greater latitudinal ranges extending frequently to latitudes $\geq 80^{\circ}$CGM. Incursion of

electron precipitation into extremely high latitudes also occurs in the evening, but much less frequently. That is, there is not the symmetry in occurrence that would be expected if B_y (positive and negative values occur at near equal frequencies) provided the principle driving mechanism.

In order to investigate the source of particles precipitating in the polar caps information on the overall state of the magnetosphere is necessary. And in particular, it is important to specify the convection electric field since it directly influences motion of low energy particles. The inner edge of plasmasheet is a direct consequence of the configuration of the magnetospheric electric field. Various theoretical models of the convection electric field exist in the literature, but direct comparison to measured values is nearly non-existent. Model predictions can be more easily tested. Specifically, the DMSP precipitating electron data give auroral equatorward boundaries which map into the inner edge of the plasmasheet. The position of the boundary is an indication of magnetospheric activity, and in particular of the strength and shape of the magnetospheric convection electric field.

This report consists of two completed studies: The first is "DMSP-F2 electron observations of equatorward auroral boundaries and their relationship to magnetospheric electric fields" and is submitted to the Journal of Geophysical Research for publication. The second is "Comment on 'Diurnal variation of the auroral oval size' by C.-I. Meng" which is currently in press at the Journal of Geophysical Research. Both studies were a collaboration with D.A. Hardy of Air Force Geophysics Laboratory, and W. J. Burke, at Boston College, and are presented as they were submitted for publication.

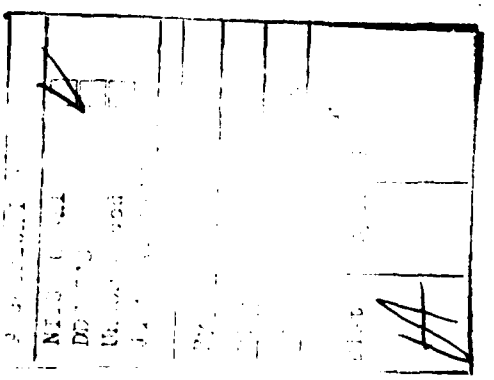

REFERENCES

Gussenhoven, M.S., Extremely high latitude auroras, AFOSR F49620-77-C-0050 Final Report, July, 1979.

Hardy, D.A., M. S. Gussenhoven, and A. Huber, The Precipitating Electron Detectors (SSJ/3) for the Block 5D/Flights 2-5 DMSP Satellites: Calibration and Data Presentation, AFGL-TR-79-0210, Hanscom AFB, MA 01731, 1979.

Heppner, J.P., Electric field variations during substorms, Planet. Sp. Sci. 20, 1475, 1972.

DMSP/F2 ELECTRON OBSERVATIONS OF EQUATORWARD AURORAL BOUNDARIES AND THEIR RELATIONSHIP TO MAGNETOSPHERIC ELECTRIC FIELDS

M.S. Gussenhoven*

D.A. Hardy+

W.J. Burke*

* Physics Department, Boston College
Chestnut Hill, MA 02167

\+ Air Force Geophysics Laboratory, Hanscom AFB
Massachusetts 07131

ABSTRACT

Energetic electron measurements from a particle detector on the DMSP/F2 satellite have been used to determine the corrected geomagnetic latitude (Λ_{CGM}) of the equatorward boundary of the auroral oval. The satellite was launched into a nearly sun-synchronous, polar orbit centered on the 0700-1900 MLT meridian. Due to the wobble of the dipole and a very slow precessional motion of the orbit more than 6000 boundary crossings could be studied in the 1600-2300 and 0400-1000 MLT sectors. The detectors, which have large geometric factors, look radially away from the earth and detect precipitating electrons with energies between 50eV and 20keV. In the evening sector the equatorward boundaries are precisely determined from the rise in the total electron flux. The morningside boundary cannot always be clearly delineated. Data were divided into one hour magnetic local time bins with ≈400 samples per bin. In each of the MLT bins Λ_{CGM} was found to be linearly correlated to the K_p index. Regression values of Λ_{CGM} were projected to the magnetic equatorial plane using the Mead-Fairfield magnetic field model. The projected boundaries are not in good agreement with the injection boundaries of Mauk and McIlwain (1974). They are best fit to boundaries derived using Volland-Stern type electric fields with the axis of symmetry rotated in the evening sector for $K_p < 2$ and into the afternoon sector for $K_p \geq 2$.

INTRODUCTION

The dynamics and sources of auroral electrons have long been of concern within the geophysical community. Whether "inverted-V" (Frank and Ackerson, 1971) electrons directly come from the magnetosheath (Frank, 1971), the magnetospheric boundary layer (Winningham et al., 1975), the neutral sheet (Speiser, 1967), or some other location in the magnetosphere remains a controversial topic. It appears to be widely accepted, however, that diffuse auroral electrons come from the central plasmasheet (Lui, et al., 1977). Thus, it is expected that the equatorward boundary of the auroral oval reflects the dynamics of the position of the inner boundary of the plasmasheet (R_p). In a general sense this appears to be true in that the equatorward boundary of the oval moves equatorward and R_p moves earthward as the level of magnetic activity increases (Vasyliunas, 1968).

Studies of the position of the equatorward boundary of the auroral oval have been conducted using imagery from the ISIS 2 (Lui, et al., 1975) and DMSP (Sheehan and Carovillano, 1978) satellites. In both instances the boundary was observed to move equatorward with increasing magnetic activity. A more comprehensive study by Kamide and Winningham (1977) used data from the soft particle spectrometers on ISIS 1 and 2 to identify the position of the boundary and to show that it shifts by $\pm 4^{\circ}$ with IMF B_z ± 5nT. The statistical sample was large enough to show that for the same value of B_z, further equatorward shifts occur 1) if a substorm is in progress, 2) during the summer, and 3) with increasing magnetic local time. A comparison of the low-latitude boundary of the oval projected into the magnetic equatorial plane with the shape of calculated zero-energy Alfvén layers (Kivelson, 1976; Southwood and Kaye, 1979)

met with mixed success. For the remainder of this paper we refer to the work of Sheehan and Carovillano (1978) and Kamide and Winningham (1977) as S-C and K-W, respectively.

The purposes of this report are to: 1) present comprehensive measurements of the corrected magnetic latitude of the equatorward boundary of the auroral oval Λ_{CGM}; and 2) compare these results to model predictions of R_P, the inner boundary of the plasmasheet. The measurements were made using an electron spectrometer on board the DMSP (Defense Metereological Satellite Program) satellite F2. In the following section we describe the instruments, the criteria for identifying Λ_{CGM}, and the methods used for binning data. It is shown that negative linear relationships exist between Λ_{CGM} and K_P in both evening and morning sectors. The discussion section is divided into three parts: 1) A comparison with ionospheric measurements of S-C and K-W is made. The comparison shows a high level of agreement between the three data sets. 2) The DMSP boundaries are projected via the Mead-Fairfield magnetic field model to the magnetic equator and compared with the injection boundaries of Mauk and McIlwain (1974). We find the agreement to be poor. 3) The boundaries are then compared to the semi-empirical model of magnetospheric electric fields of Volland (1974) and Stern (1975). The best fits to DMSP observations are found using shaping factors between 2 and 3 and with the axis of symmetry rotated away from the dawn-dusk meridian.

INSTRUMENTATION AND DATA SELECTION

DMSP/F2 is a three-axis stabilized satellite in a near sun-synchronous, circular orbit at an altitude of 840 km. The orbital period is 101 minutes; the nominal inclination is 98.75°. At launch the orbit was centered near the 0700-1900 meridian but is subject to a very slow precession toward later local times. Due to the offset between the earth spin axis and magnetic axis, the

orbit is subject to significant diurnal and seasonal variations in the magnetic local time-magnetic latitude frame of reference. Thus, Λ_{CGM} is sampled in a wider range of MLT than might be assumed from the restricted geographic local time locations of the orbit. It should also be noted that DMSP is an operational Air Force satellite. Except during periods of down-link transmissions, data are almost always being recorded.

The particle detector on DMSP/F2 consists of two curved plate electrostatic analyzers that measure the fluxes of electrons in 16 energy channels between 50eV and 20keV once per second. The apertures of the analyzers always face local vertical such that at auroral and polar cap latitudes they detect precipitating rather than back scattered and/or trapped electrons. One analyzer covers the energy range from 50eV to 1keV with a geometric factor of $4 \times 10^{-4} cm^2$ ster and a $\Delta E/E$ of 10 percent. The other analyzer covers the energy range from 1keV to 20keV with a geometric factor of $10^{-3} cm^2$ ster and a $\Delta E/E$ of 12 percent. The large geometric factors insure that the flux level for the electrons in the diffuse aurora is well above the detector's sensitivity. A detailed description of the detector is given by Hardy et al. (1979).

An example of DMSP/F2 electron data, taken from a south polar pass on 2 July, 1977 is given in Figure 1. Data are plotted as JTOT, the directional integral flux $(cm^2 ster\ sec)^{-1}$ in the bottom panel; JETOT, the directional energy flux $(keV/cm^2 ster\ sec)$ in the middle panel, and EAVE, the average energy in keV in the top panel. The scale for EAVE is linear. These quantities are plotted as functions of universal time in seconds of the day; the geographic latitude and longitude of the subsatellite position; the corrected geomagnetic latitude and longitude of the satellite projected to an altitude of 100 km; and the magnetic local time. Values of the equatorial boundaries (Λ_{CGM}) of the auroral oval are assigned to the corrected geomagnetic latitudes $>45^{\circ}$

at which JTOT rises noticeably above background. This is essentially the same method used by Kamide and Winningham (1977). In the example given in Figure 1, Λ_{CGM} is at -66.6° on the evening side (∿20MLT) and at -65.1° on the morning side (∿07MLT).

Several characteristics of the electron precipitation that pertain to the choice of auroral boundaries are illustrated in Figure 1. First, we have found the condition JTOT>10^7 $(cm^2 ster\ sec)^{-1}$, indicated in the figure by the horizontal line, provides a generally useful criterion for selecting both the poleward and equatorward boundaries of the oval. The poleward boundaries selected in the case given in Figure 1 are marked for purposes of illustration. They and their attendant selection problems will not be discussed here. Second, the evening equatorward boundary is sharper than its morningside counterpart. On the morning side JTOT rose from background to 10^7 $(cm^2 ster\ sec)^{-1}$ over 1.4° latitude, whereas the evening side rise was nearly instantaneous. Generally, flux gradients are found near both equatorward boundaries. The gradient never extends more than a few degrees latitude in the evening sector, but can cover as much as 10° on the morning side where it is always perceptibly present. Third, equatorward of the evening and morning values of Λ_{CGM} there are slight rises in JTOT with relatively large values of JETOT and EAVE. These increases are due to radiation belt particles that penetrate the detector casing and directly stimulate the channeltrons; they must be differentiated from the auroral electrons when determining boundaries. Due to the geometrical configurations of the two detectors, radiation belt contamination is largely limited to the energy channels of the 1 to 20 keV detector.

The boundary of the oval, Λ_{CGM}, cannot always be determined unambiguously. On both morning and evening sides of the oval, the onset of electron precipitation can be obscured in various ways. In the evening the principle problem

is contamination of the low energy channels of the detector by photoelectrons. As an example in Figure 2 we have plotted the count rates in representative channels of the detector as a function of increasing geographic latitude. Arrows show where there is a significant increase in counts due to the onset of precipitating auroral electrons. The increase in counts is observed first in the lowest energy channel and then, progressively, in higher energy channels. In the 50eV channel significant counts are observed equatorward of the arrow. These counts arise from photoelectrons from the conjugate ionosphere. The effect of photoelectrons can be observed at energies as high as several hundred electron volts. Since the photoelectrons are observed in the same channels as the onset of precipitation, the ambiguity in the boundary is introduced by having to separate the two effects. Also shown in Figure 2 are increased counts in the 5.5keV channel equatorward of auroral electron precipitation. This is an example of radiation belt contamination. As discussed above the effect is seen only in the channels of the high energy detector. In the evening sector, auroral precipitation is first detected in the lowest energy channels. At times when the radiation belt and the auroral oval overlap the combination of high energy channel contamination and increased low energy count rates produces an increase in JTOT and a decrease in EAVE. Thus, the auroral boundary determination is unaffected.

Uncertainties in identifying the position of the boundary in the morning sector are more severe. There are three sources of uncertainty: 1) overlap between regions of energetic electron precipitation and radiation belt contamination of corresponding energy channels; 2) a much more gradual latitudinal onset of precipitation than is found in the evening, and 3) the existence of energetic plasma close to but detached from the boundary. In

Figure 3 we have plotted for the morning auroral zone the counts as in Figure 2. The figure shows that for this case the onset of electron precipitation in the morning appears first in the high energy channels and then progressively in lower energy channels. For this case the region in which penetrating particles are producing counts are equatorward of the onset of auroral precipitation. In active periods they can overlap. Since the count levels are comparable, for the cases of overlap it is difficult to separate the two effects and our ability to determine the boundary is affected.

The second effect causing ambiguity in identifying the morningside boundary is illustrated in Figure 4 which shows a complete south polar pass from 28 February, 1978. On the morning side a gradient in JTOT continues into the region of radiation belt contamination. JETOT and EAVE fall sharply at -64.7^{o}CGM but JTOT remained too high to be explained as contamination until -58.5^{o}. At -58.5^{o} EAVE rose with significant scatter indicating the presence of dominant radiation belt contamination and obscuring the possible presence of keV electron precipitation. In cases such as this the boundary was chosen to be at the lowest magnetic latitude at which precipitating electrons could be identified; in this case $\Lambda_{CGM} = -58.5^{o}$.

The third effect which can be found in both morning and evening regions is shown in Figure 5. This example shows a north pole pass on January 21, 1977, during a time of magnetospheric quiet. On the evening side there are small regions of energetic electrons near to but detached from the more poleward precipitation region. These can occur during active times, as well, and are ignored in selecting the boundaries.

The above effects produced greater than 1 degree uncertainty in the equatorial boundary only for a small percentage of the total cases. On the

evening side approximately 90 percent of boundaries were determined with no ambiguity. On the morning side the figure was approximately 70 percent.

More than 6000 auroral oval boundary crossings were determined using data from September, 1977 to December, 1978. Over two-thirds of the crossings occurred during north pole Fall and Winter months. It was necessary to use Spring and Summer data to obtain a good statistical sample for high K_p values. The measurements are binned into one hour units of MLT and to all steps in K_p (0, 0^+, 1^- ...). Cases were selected to insure that 20 to 25 samples were included in each $K_p \leq 6$ element. In some MLT sectors a statistically significant number of samples were available for $K_p > 6$ elements. Due to the orbital characteristics of DMSP/F2 these criteria were largely met in the 17-23 and 04-10 MLT sectors of the northern hemisphere and the 17-21 and 04-08 sectors of the southern hemisphere. The major exceptions were the 18-19 MLT sector of the northern hemisphere in which only 103 samples were found, and the 15-16 MLT sector in the southern hemisphere having 107 samples. The small sample size resulted from the fact that the DMSP/F2 orbit drifted slowly out of (into) these regions over the time interval used.

OBSERVATIONS

Examples from the evening (19-20) and morning (07-08) MLT sectors in which coverage is available from both the northern (top traces) and southern (bottom traces) hemispheres are given in Figures 6 and 7. The average value and the standard deviation of the boundaries within each K_p bin is shown. Solid lines represent linear regressions perfor ed with all the points in the MLT sector versus K_p (not with the mean values). The equation for the line is given in the upper right hand corner of each plot. The correlation coefficient (cc) is also given.

From an examination of data contained in these figures several points can be made: 1) K_p orders the equatorward auroral boundaries linearly throughout the entire range. The mean values lie on or very near the line. The fit is exceptional for the evening values, and while there is more variation in the morning, no trend other than linear is apparent. The correlation coefficients across the whole K_p range are very high: $\leq -.81$ for the four cases shown. 2) Standard deviations about mean values tend to increase with increasing K_p. Also, standard deviations in the morning sector are greater than those found in the evening sector. This reflects our general observation that auroral electron precipitation patterns are far more variable in the morning than evening sector. 3) In MLT regions of overlap Λ_{CGM} has lower values in the southern hemisphere. The difference is greater in the morning for low K_p values. The slopes in the straight line fit have larger negative values in the north pole, and the difference between the boundaries approaches zero for large K_p. The difference may be due to north-south assymmetries in mirror points of plasmasheet electrons. It may also reflect a summer-winter assymmetry due to the tilt of the dipole noted by Kamide and Winningham (1977). Recall that most of the data points used in the present study were acquired within three months of the December 1977 solstice.

The entire data set is summarized for the morning and evening sectors in Tables 1 and 2, respectively. Here we have listed values of Λ_o and α calculated from the regression formula: $\Lambda_{CGM} = \pm(\Lambda_o + \alpha K_p)$, where the +(-) sign refers to the north (south) pole. Also listed are the number of cases, N, and the correlation coefficient, cc. Even including the MLT sectors for which the statistical sample was small the correlation coefficients lie in the range $-.58 \geq cc \geq -.90$. For the full samples correlation coefficients

were less than -.7 in the morning and less than -.8 in the evening. This suggests that K_P is better for organizing Λ_{CGM} than IMF B_z. Correlation coefficients reported by K-W were in the $-0.4 \geq cc \geq -0.7$ range. Evening sector values of Λ_{CGM}, for a given value of K_P decreased with increasing MLT. According to K-W this decrease continues into the post-midnight sector. In the dawn sector Λ_o increases with increasing MLT. However, at $K_P = 6$ dawn and post-dawn sector values of Λ_{CGM} approach a constant value of $\sim 57^o$. Values of α in the evening sector fall in the restricted range -1.6 ± 0.4, and -1.75 ± 0.4 in the morning sector. The largest negative values of α were at 07-08 MLT and 18-19 MLT, indicating that the greatest variability in the boundaries occurs near dawn and dusk.

DISCUSSION

A. COMPARISON WITH MEASURED IONOSPHERIC BOUNDARIES

Direct quantitative comparisons of results presented in the previous section with the work of S-C and K-W are not possible for many reasons. Correlated quantities were not the same and were sampled largely in different MLT sectors. S-C used optical rather than particle signatures to identify the corrected magnetic latitude of the equatorward boundary as a function of K_P. K-W studied the invariant latitude of the boundary as a function of IMF B_z. Although B_z influences geomagnetic activity, its relationship with K_P is not a simple one. However, some semi-qualitative comparisons of the various results can be made if we assume that times when $B_z = +(-)5$ correspond to periods of low (high) geomagnetic activity. With these simplifying assumptions we have plotted in Figure 8 "values" of Λ_{CGM} observed by the various DMSP and ISIS satellites for periods of magnetic quiet and disturbance. Symbols θ and

X refer to DMSP/F2 northern and southern hemisphere observations, respectively. The high (low) latitude points were calculated for cases of K_p = 0 (5) using regression coefficients of Tables 1 and 2. The Δ symbols refer to boundary values calculated using regression coefficients given in Table 1 of K-W with $B_z = \pm 5\gamma$. The ◻ symbols refer to measurements at MLT = 01, 20, and 22 for K_p = 0 and 5 as taken from Figure 2 and 8 of S-C.

The auroral boundary derived from the three data sets for periods of magnetic quiet shows a remarkable consistency. In MLT sectors of common measurements the quiet time results are within 1^o of each other. The boundary appears to be continuous across the entire night side. The one anomalous point in the 03-04 MLT sector was based on a data set of 8 points and is virtually without statistical signficance. It is interesting to note that Meng et al. (1977) have shown that the poleward boundary of the quiet auroral oval can be represented by an offset circle. During magnetically quiet times the oval tends to be of narrow latitudinal width. Perhaps not surprisingly Λ_E can also be well fit to an offset circle. (The symbol Λ_E is used in comparing DMSP with equatorward boundaries of S-C and K-W rather than the symbol Λ_{CGM} which is reserved for DMSP/F2 data alone.) In Figure 8 the quiet time boundary is fit to a circle of radius 21^o that is centered at 88.0^o and 02.7 MLT (dashed line). DMSP/F2 values fall within the circle at 18-20 MLT and 06-08 MLT, deviations which will later be shown to have significance.

At times of high geomagnetic activity agreement between the data sets is not as good. The boundary for K_p = 5 derived from DMSP/F2 measurements is smooth in the evening and morning sectors. The high activity boundaries from S-C and K-W are mutually consistent but are displaced poleward of F2 results by 2^o in the pre-midnight region. No comparison is possible for the post-midnight

region. Variation from S-C data can be accounted for as a difference between optical and particle boundaries. On the other hand, in their analysis K-W noted that for the same value of B_z the value of Λ_E could be shifted equatorward by several degrees if a substorm was in progress. During times of $K_p = 5$ it is expected that substorms would almost always be in progress. Examining the distribution of points in Figure 3a of K-W, we see that in the 20-21 MLT sector for $B_z = -5nT$, Λ_E was observed at 61^o and 59^o where the regression value is 63^o. In general, most of K-W's data points taken during times when substorms were in progress lie well below the regression line. Evidently, the value of Λ_E reflects the dynamic state of the magnetosphere which depends on physical parameters other than just the hourly average of B_z.

B. COMPARISON WITH MAGNETOSPHERIC BOUNDARIES

The notion of an injection boundary was first proposed by Mauk and McIlwain (1974) to systematize magnetic local times (ϕ) at which the ATS-5 satellite at $6.7R_E$ encountered sharp increases in low energy (keV) plasma fluxes as a function of K_p. A least squares regression analysis gave the relationship

$$\phi\ (L = 6.7) = 25.5 - 1.5\ K_p\ (K_p \leq 5^+) \quad . \qquad (1)$$

To extend these points and to give a generalized plasma boundary Mauk and McIlwain used Carpenter and Park's (1973) relationship between the position of the plasmapause at $\phi = 0600$ (L_D) and K_p; $L_D = 5.7 - .47\ K_p$. The Carpenter and Park relationship was derived using the highest values of K_p in the previous 24 hours rather than its current value. Mauk and McIlwain assumed that the shape of the boundary was of the form

$$L(\phi, K_p) = \frac{SL_D}{(\phi + C)} \quad . \qquad (2)$$

By forcing the boundary to pass through L = 6.7 at local times specified in (1) it can be shown that the constants S and C have values of 21.4 and -7.3, respectively.

The term injection boundary is not without ambiguity (Kivelson et al. 1978). It may either signify a dynamic plasma boundary which is suddenly pushed earthward to the position of the satellite or refer to a quasi-static boundary that is crossed by the satellite. In the dynamic case the electron flux shows little or no energy-time dispersion. In the quasi-static case electrons are first detected at low energies, then at higher energies as the satellite penetrates further into the boundary. Kivelson et al. (1978) have suggested that this energy-time dispersion is characteristic of the satellite crossing the Alfvén boundaries of electrons with higher and higher energies. As discussed below, Alvén boundaries mark boundaries between open and closed magnetospheric trajectories for particles of given charge and magnetic moment. The zero energy Alfvén layer is thus the boundary between open and closed equipotential surfaces in the magnetosphere. For the remainder of this paper, we treat quasi-static injection boundaries and Alfvén layers as equivalent concepts.

The energy-latitude dispersion shown in Figure 2 to be characteristic of the equatorward edge of auroral precipitation in the evening sector is precisely what would be expected from mapping a quasi-static injection boundary into the ionosphere, and gives credance to our association of the DMSP/F2 boundaries with the inner edge of the established plasma sheet. A quasi-static injection boundary R_p can be determined from Λ_{CGM} by mapping these

latitudes into the equatorial plane where comparison can then be made to the Mauk-McIlwain injection boundary.

Before making this comparison, several points should be kept in mind. First, the mapping is extremely sensitive to magnetic field models, and small variations in Λ_{CGM} appear as large variations in L-shell. Figure 9 illustrates both of these points. Here we have mapped the best circle fit to the quiet auroral oval shown in Figure 8 onto the equatorial plane using a) a dipolar projection (dashed line) and b) a projection using the Mead-Fairfield magnetic field model for $K_p < 2$ (solid line). (See Fairfield and Mead, 1975). The difference between the two can be as large as $2R_E$ in the evening sector. Also shown in Figure 9 is the best smooth fit to the data points, Λ_{CGM}, mapped using the Mead-Fairfield magnetic field (dash-dot line). The north and south pole values are averaged for overlapping MLT sectors. The small deviation of Λ_{CGM} from the circular fit in the 18-20 MLT sector, which was pointed out previously results in a significant boundary change in the equatorial plane.

Because the representation of the Mauk-McIlwain boundary given in (2) is valid only at local times prior to 0200 comparisons with DMSP/F2 boundaries are limited to the evening sector. We can, however, directly compare the DMSP/F2 boundary with Carpenter and Park's (1973) plasmapause measurements at dawn. Figure 10 shows this comparison. The DMSP values are calculated from averages of Λ_{CGM} in the 05-06 and 06-07 MLT sectors. The inner edge of the plasmasheet as determined by DMSP/F2 auroral boundaries lies beyond the plasmapause, asymptotically approaching a constant separation of $\sim 0.3R_E$ for large K_p. This separation is within that of the standard deviation in Λ_{CGM}. The deviation from linearity for small K_p cannot be accounted for in this way and indicates that the assumption: $L \propto L_D$ in (2) for a given local time, is a poor one for low K_p.

Figure 11 compares the Mauk-McIlwain injection boundaries (dashed lines) for K_p = 0, 2 and 5, to the inner edge of the plasmasheet as determined from Λ_{CGM} values for the same K_p levels (solid lines). For K_p 2 and 5 the Mauk-McIlwain injection boundaries lie within the plasmasheet. This is consistent with photometric auroral observations at the foot of the ATS5 field line by Eather et al. (1976). They found that substorm related injections occurred within the existing plasmasheet in the pre-midnight sector. These injections were furthest from R_p at dusk and approached R_p near midnight. Mauk-McIlwain statistics include all injection boundaries encountered, a mix of dynamic and quasi-static boundaries. The boundary that results (R_{M-M}) should then lie within the plasmasheet, or at $R_{M-M} > R_p$. This is the relationship the Mauk-McIlwain boundary has to the DMSP/F2- determined boundary for K_p = 2-5; with $R_{M-M} \rightarrow R_p$ near midnight.

For K_p = 0, the two boundaries differ greatly, particularly in the evening sector. The local time at which ATS-5 statistically crosses the quiet-time injection boundary is 0130, which point compares very favorably with the inner edge of the plasmasheet as measured by DMSP/F2. Using higher values for the inner edge of the plasmasheet at dawn than those given by Carpenter and Park will expand the Mauk-McIlwain boundary, but the essentially different shape of the DMSP/F2 boundary indicates that for low K_p values the Mauk-McIlwain boundary is valid over a very restricted local time range. This is not surprising since geosynchronous orbits rarely enter the plasma sheet during very quiet times, and when they do, it is post-midnight, far from the dusk boundary in question.

C. A QUASI-EMPIRICAL REPRESENTATION OF THE OBSERVED BOUNDARIES

Charged particles in the magnetosphere are subject to gradient-curvature and to $\underline{E} \times \underline{B}$ drifts. The gradient-curvature drift depends on the charge and

energy of the particle while the electric field drift does not. The electric field is a superposition of the general dawn to dusk convective field, the corotation field and fields due to charge separations within the system. The latter type of field is primarily due to shielding charges near the plasmapause (Jaggi and Wolf, 1973) and to polarization charges at conductivity gradients near the terminator in the ionosphere (Wolf, 1970). The shape and position of magnetospheric boundaries for low energy plasmasheet electrons under the assumption of a uniform cross-tail electric field has been discussed by Kivelson (1976). The electrons drift earthward from the tail along equipotential surfaces, then eventually exit the magnetosphere across the dayside magnetopause. The zero energy Alfvén boundary delineates regions of allowed and forbidden access. Its characteristic teardrop shape is that of the last closed equipotential. Based on electric field measurements at ionospheric altitudes (Heppner 1972), Volland (1973) and Stern (1975) suggested that the convective field is not uniformly dawn to dusk. Ejiri et al. (1978) derived an analytic expression for the zero energy Alfvén boundary under nonuniform electric field situations that uses a shaping factor γ. Recently Kaye (1980) suggested that the value of γ reflects the degree to which space charges shield the convective electric field from the inner magnetosphere. The case $\gamma = 1$ corresponds to situations of uniform dawn to dusk fields in which there is no shielding. The major effect of the near-terminator conductivity gradient is to rotate the dusk bulge of the Alfvén boundary into the evening sector (Wolf, 1970).

In the equatorial plane of the magnetosphere the potential from which the total electric field is derived is assumed to be of the form:

$$\Phi(R,\phi) = -\frac{\Omega B_o R_E^3}{R} + AR^{\gamma}\sin(\phi - \phi_o) \quad , \tag{3}$$

where Ω is the angular spin velocity of the earth, B_o the magnetic field strength at the magnetic equator on the earth's surface, R is the distance from the center of the earth and ϕ is the local time measured counter-clockwise from midnight. The phase angle, ϕ_o, represents the rotation of the axis of symmetry away from the dawn-dusk meridian. The boundary between open and closed equipotentials is calculated by assuming that at a distance R_S and a local time $\phi - \phi_o = 3\pi/2$, the convection and corotational electric fields cancel each other. The condition that $\partial\Phi/\partial R = 0$ at this point allows a determination of the constant $A = \frac{\Omega B_o R_E^3}{\gamma R_S^{(\gamma+1)}}$. Following Ejiri et al. (1978) it is easily shown that the equation for the boundary is:

$$\left[\frac{R_P}{R_S}\right]^{\gamma+1} \sin(\phi - \phi_o) + (\gamma + 1)\frac{R_P}{R_S} - \gamma = 0 \quad . \tag{4}$$

Southwood and Kaye (1979) have shown that an excellent approximation to the solution of (4) is

$$R_P \simeq R_S\left(1 + \frac{\sqrt{2}s}{\gamma}\right)^{-1} \quad , \tag{5}$$

where $s = \left|\cos\left[\frac{90 - (\phi - \phi_o)}{2}\right]\right|$. For $\gamma = 1$ the solution is exact. The boundary has a tear-drop shape, becoming less eccentric for higher values of γ.

From the shape of the boundary illustrated in Figure 9 it is obvious that the axis of symmetry for the equatorial projection of the DMSP/F2 measured boundary is not the dawn-dusk meridian; i.e. $\phi_o \neq 0$. The degree of rotation from the dawn-dusk meridian as well as the shapes of the boundary in the $0 \leq K_p \leq 5$ range are given in Figure 12. For $K_p = 0$ and 1 the rotation is counterclockwise by 23^o and 8^o, respectively. For $K_p = 2$, 3 and 5 the axis of symmetry is rotated clockwise (into the afternoon local time sector) by approximately 30^o, 45^o and 45^o respectively. The exact degree of clockwise

rotation cannot be determined at this time because of the absence of DMSP/F2 data in the afternoon and postmidnight sectors. The rotation of the boundary's axis of symmetry into the evening sector at times of low K_p is due to ionospheric charge pile up near the day-night terminator (Wolf, 1970). Increasing particle precipitation at times of high K_p weakens the ionospheric conductivity gradient near the terminator. It is thus expected that for higher K_p the axis would rotate back toward the dawn-dusk meridian. The physical basis for a strong rotation of the symmetry axis into the afternoon sector for $K_p \geq 2$ is not yet understood.

Figure 12 also shows results of fitting the zero energy Alfvén boundary for $\gamma = 2$ and 3 using empirical values of ϕ_o. The method used for deriving the boundary values is as follows: 1) Data points marked by the symbol Θ are obtained for a given K_p using regression coefficients from Tables 1 and 2. Where north and south data sets overlap in local time, average boundary values are used. The Mead-Fairfield model is then used to map points into the equatorial plane. 2) Because the boundary represented by (4) gives a shape but not a distance for a given value of γ, the data points closest to the boundary minimum (i.e. opposite the dusk side stagnation point) are used to 'anchor' the boundary. This procedure is justified because the radial distance of the boundary varies slowly in the morning local time sector and the boundary shape is nearly the same for all values of γ. Boundaries derived for the $\gamma = 1$ case are not shown in Figure 12 because their stagnation points lie well outside the $\gamma = 2$ values. Dashed lines representing the Mauk-McIlwain boundaries are provided for reference. The data points in Figure 12 lie close to the $\gamma = 2$ and $\gamma = 3$ curves with a tendency toward slightly lower values of γ for higher values of K_p. Values of γ between 2 and 3 are in agreement with a variety of equatorial observations reported by Ejiri et al. (1978), Southwood and Kaye (1979), and Hughes et al. (1979). Kaye (1980) suggested that the

tendency toward lower values of γ with increasing K_p reflects a more dynamic mangetosphere in which shielding layers do not have sufficient time to become fully developed. This hypothesis awaits DMSP data acquisition in the afternoon sector for its verification.

Data presented in Figure 12 can also be used to provide a useful, empirical expression for the electrostatic potential. Equation (3) can be written:

$$\Phi(L,\phi) = \Omega B_o R_E^2 \left[\frac{L^\gamma}{\gamma L_S^{\gamma+1}} \sin(\phi - \phi_o) - \frac{1}{L} \right], \tag{6}$$

where $L = R/R_E$ and $L_S = R_S/R_E$. It is useful to define a parameter $\xi = 1/L_S^{\gamma+1}{}_\gamma$. Using stagnation distances derived from Figure 12 as a function of K_p a linear relationship

$$\xi = (3.9 + 6.0K_p) \cdot 10^{-5} \quad (cc = 0.97), \tag{7}$$

was found for the case $\gamma = 2$. In the case $\gamma = 3$, the quadratic relationship

$$\xi = (8.0 + 4.4\ K_p)^2 \cdot 10^{-5} \quad (cc = 0.99)\ , \tag{8}$$

was found. Thus for the case $\gamma = 2$ the total potential is

$$\Phi(L,\phi) = \Omega B_o R_E^2 \left[(3.9 - 6.0K_p) \cdot 10^{-5}\ L^2 \sin(\phi - \phi_o) - \frac{1}{L} \right]\ . \tag{9}$$

It should be recalled that ϕ_o is a function of K_p that is not describable in a simple analytic form.

SUMMARY

By associating the equatorward boundaries of auroral electron precipitation as measured by DMSP/F2 satellite with the inner edge of the plasmasheet in a very large statistical sample, we find:

1) K_p orders the data well, particularly in the evening sector. In a given MLT sector, the latitude of the equatorward edge of the precipitation decreases linearly with K_p, indicating that the inner edge of the plasmasheet moves earthward.

2) The inner edge of the plasmasheet is earthward of the Mauk-McIlwain injection boundary for $K_p \geq 2$.

3) The inner edge of the plasmasheet is not symmetrical about the dawn-dusk axis, but is symmetrical about an axis whose angle to the dawn-dusk axis depends on K_p, reaching a constant value at $K_p = 3$. That is, the cross tail electric field is not always dawn to dusk but has an anti-sunward component for low K_p and a sunward component for $K_p \geq 2$.

4) The inner edge of the plasmasheet can be modelled as the zero-energy Alfvén layer in a magnetosphere whose large-scale electric field is obtained from a Volland-Stern potential with $\gamma \geq 2$. For $\gamma = 2$, the K_p dependence of the potential is found to be:

$$\Phi = \mathcal{R}B_o R_E^2 \left[(3.9 - 6.0K_p) \cdot 10^{-5} L^2 \sin(\phi - \phi_o) - \frac{1}{L} \right] .$$

Here, ϕ is dependent on K_p as well, but is not easily described analytically.

ACKNOWLEDGEMENTS

The authors are grateful to Nancy Heinemann, Deborah L. Gustafson, and Joan Hogan for the great care and consistency with which they made the boundary determinations from the DMSP/F2 data. They also wish to thank Richard McKeen for completing the programming associated with this work. This work was supported by the Air Force Office of Scientific Research under Research Grant AFOSR-79-0012 and by Air Force Geophysics Laboratory Contract F19628-79-C-0031.

REFERENCES

Carpenter, D. L. and G. G. Park, On what ionospheric workers should know about the plasmapause - plasmasphere, Rev. Geophys. Sp. Phys. 11, 133, 1973.

Fairfield, D. H. and G. D. Mead, Magnteospheric mapping with a quantitative geomagnetic field model, J. Geophys. Res., 80, 535, 1975.

Frank, L. A., Comments on a proposed magnetospheric model, J. Geophys. Res., 76, 2512, 1971.

Frank, L. A. and K. L. Ackerson, Observations of charged particle precipitation in the auroral zone, J. Geophys. Res., 76, 3612, 1971.

Eather, R. H., S. B. Mende, R. J. R. Judge, Plasma injection at synchronous orbit and spatial and temporal auroral morphology, J. Geophys. Res., 81, 2805, 1976.

Ejiri, M., R. A. Hoffman and P. H. Smith, The convection electric field model for magnetosphere based on Explorer 45 observations, J. Geophys. Res., 83, 4811, 1978.

Hardy, D. A., M. S. Gussenhoven, and A. Huber, The Precipitation Electron Detectors (SSJ/3) for the Block 5D/Flights 2-5 DMSP Satellites: Calibration and Data Presentation, AFGL-TR-79-0210, Hanscom AFB, MA 01731, 1979.

Heppner, J. P., Electric field variations during substorms, Planet. Sp. Sci. 20, 1475, 1972.

Hughes, W. J., R. L. McPherron, J. N. Barfield, and B. H. Mauk, A compressional Pc4 pulsation observed by three satellites in geostationary orbit near local midnight, Planet. Sp. Sci., 27, 821, 1979.

Jaggi, R. K. and R. A. Wolf, Self-consistent calculation of the motion of a sheet of ions in the magnetosphere, J. Geophys. Res., 78, 2852, 1973.

Kaye, S. M., Determination of the magnitude of the convection electric field measurements, Yosemite High Latitude Electric Field Conference, Jan. 30-Feb. 2, 1980.

Kamide, Y. and J. D. Winningham, A statistical study of the "instantaneous" nightside auroral oval: the equatorial boundary of electron precipitation as observed by the Isis 1 and 2 satellites, J. Geophys. Res., 82, 5573, 1977.

Kivelson, M. G., Magnetospheric electric fields and their variations with geomagnetic activity, Rev. Geophys. Sp. Phys., 14, 189, 1976.

Kivelson, M. G., S. M. Kaye and D. J. Southwood, The physics of plasma injection events, presented at AGU Chapman Conference on Magnetospheric Substorms, Los Alamos, NM, 1978.

Lui, A. T. Y., C. D. Anger and S.-I. Akasofu, The equatorward boundary of the diffuse aurora and auroral substorms as seen by the Isis 2 auroral scanning photometer, J. Geophys. Res., 80, 3603, 1975.

Lui, A. T. Y., D. Venkatesan, C. D. Anger, S.-I. Akasofu, W. J. Heikkila, J. D. Winningham and J. R. Burrows, Simultaneous observations of particle precipitation and auroral emissions by the Isis 2 satellite in the 19-24 MLT sector, J. Geophys. Res., 87, 2210, 1977.

Mauk, B. H. and C. E. McIlwain, Correlation of K_P with substorm injected plasma boundary, J. Geophys. Res., 79, 3193, 1974.

Meng, C.-I., R. H. Holzworth and S.-I. Akasofu, Auroral circle delineating the poleward boundary of the quiet auroral oval, J. Geophys. Res. 82, 164, 1977.

Sheehan, R. E. and R. L. Carovillano, Characteristics of the equatorward auroral boundary near midnight determined from DMSP images, J. Geophys. Res., 83, 4749, 1978.

Southwood, D. J. and S. M. Kaye, Drift boundary approximations in simple magnetospheric convection models, J. Geophys. Res., 84, 5773, 1979.

Speiser, T. W., Particle trajectories in model current sheets, II: Application to auroras using a geomagnetic tail model, J. Geophys. Res., 72, 3919, 1967.

Stern, D. P., The motion of a proton in the equatorial magnetosphere, J. Geophys. Res., 80, 595, 1975.

Tsurutani, B. T. and E. J. Smith, Two types of magnetospheric ELF auroras and their substorm dependence, J. Geophys. Res., 80, 5112, 1977.

Vasyliunas V. M., A survey of low energy electrons in the evening sector of the magnetosphere with OGO 1 and OGO 3, J. Geophys. Res., 73, 2839, 1968.

Volland, H., A semiempirical model of large scale magnetospheric electric fields, J. Geophys. Res., 78, 171, 1973.

Winningham, J. D., F. Yasuhara, S.-I. Akasofu, and W. J. Heikkila, The latitudinal morphology of 10-eV to 10-keV electron fluxes during magnetically quiet and disturbed times in the 2100-0300 MLT sector, J. Geophys. Res., 80, 3148, 1975.

Wolf, R. A., Effects of ionospheric conductivity on convective flow of plasma in the magnetosphere, J. Geophys. Res., 75, 4677, 1970.

FIGURE CAPTIONS

Figure 1. The integral flux in $(cm^2 ster\ sec)^{-1}$ (bottom panel), energy flux in keV $(cm^2 ster\ sec)^{-1}$ and average energy in keV (top panel) of precipitating electrons measured by the DMSP/F2 satellite passing over the south pole on July 2, 1977. These are plotted as functions of universal times (in seconds); geographic latitude and longitude of the sub-satellite position; corrected geomagnetic latitude and longitude of the satellite position projected along a Jensen-Cain magnetic field to 100 km; and magnetic local time. The vertical lines indicate equatorward and poleward boundaries of precipitating auroral electrons.

Figure 2. Counts in selected channels of the SSJ/3 detector plotted as a function of increasing geographic latitude for a pass over the evening side auroral zone boundary.

Figure 3. As in Figure 2, for a pass over the morning side auroral zone boundary.

Figure 4. Precipitating electron data for a south pole pass on February 28, 1978. The format is the same as in Figure 1.

Figure 5. Precipitating electron data for a north pole pass on January 21, 1977. The format is the same as in Figure 1.

Figure 6. Mean values and standard deviations of equatorward boundaries in each K_p line plotted as a function of K_p for north and south poles in the 19-20 MLT sector. The solid line results from a linear regression performed using individual boundary determinations. Linear regression results are summarized for given Kp ranges.

Figure 7. As in Figure 6 for the 07-08 MLT sector.

Figure 8. Equatorward boundary of auroral oval as a function of MLT for high and low levels of magnetic activity. Data marked by symbols Θ, X, Δ, and □ come from north and south hemisphere measurements of DMSP/F2 (K_p = 0, 5) measurements of ISIS ($B_z = \pm 5\gamma$) and DMSP optical imagery (K_p = 0, 5) respectively. The quiet time oval has been fit to an offset circle (dashed line).

Figure 9. Projections of the circular fit of K_p = 0 boundaries to the ecliptic plane using a dipolar projection (dashed line); the Mead-Fairfield magnetic field model (solid line). The dash-dot curve is the projection by means of a Mead-Fairfield magnetic field model of a smooth fit to the individual boundary values for K_p = 0.

Figure 10. A comparison of the Carpenter-Park values of the plasmapause at dawn to the inner edge of the plasmasheet at dawn as determined by the DMSP/F2 boundaries.

Figure 11. A comparison of the inner edge of the plasmasheet as determined by the DMSP/F2 boundaries to the Mauk-McIlwain injection boundaries for various K_p.

Figure 12. Volland-Stern injection boundaries for $\gamma = 1$ and $\gamma = 2$ rotated to fit the inner edge of the plasmasheet as determined by the DMSP/F2 auroral boundaries, for various K_p. The Mauk-McIlwain injection boundary is also shown (dashed line).

	NORTH				SOUTH				
MLT	Λ_o	α	N	cc	MLT	Λ_o	α	N	cc
04-05	67.4	-1.35	171	-.58	04-05				
05-06	67.8	-1.87	365	-.75	05-06				
06-07	68.5	-1.96	403	-.82	06-07	67.4	-1.67	376	-.74
07-08	70.2	-2.15	367	-.83	07-08	68.3	-1.97	411	-.81
08-09					08-09	68.7	-1.88	302	-.72
09-10					09-10	69.1	-1.64	217	-.67

TABLE 1

	NORTH				SOUTH				
MLT	Λ_o	α	N	cc	MLT	Λ_o	α	N	cc
16-17	-	-	-	-	16-17	71.3	-1.19	107	-.65
17-18	-	-	-	-	17-18	70.7	-1.20	256	-.69
18-19	71.6	-2.00	103	-.90	18-19	70.6	-1.60	327	-.80
19-20	71.2	-1.96	426	-.89	19-20	70.0	-1.82	447	-.87
20-21	69.4	-1.85	452	-.82	20-21	69.5	-1.89	345	-.84
21-22	68.7	-1.66	556	-.83	21-22	-	-	-	-
22-23	68.3	-1.79	184	-.63		-	-	-	-

TABLE 2

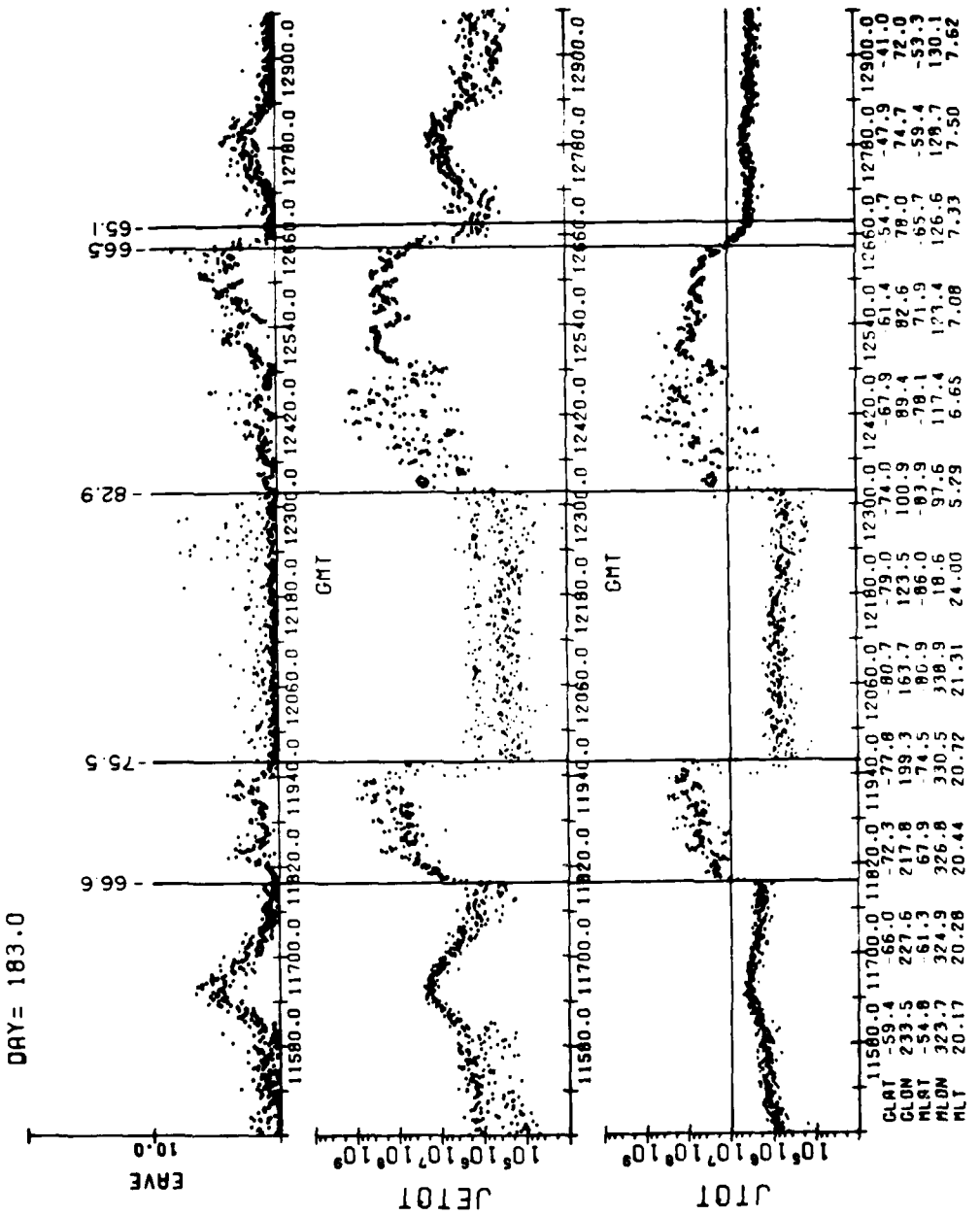
DAY= 183.0
EAVE
JETOT
JTOT
GMT
GMT
65.1
66.5
82.9
75.5
66.6
11580.0 11700.0 11820.0 11940.0 12060.0 12180.0 12300.0 12420.0 12540.0 12660.0 12780.0 12900.0
CLAT -59.4 -66.0 -72.3 -77.8 -80.7 -79.0 -74.0 -67.9 61.4 -54.7 -47.9 -41.0
CLON 233.5 227.6 217.8 199.3 163.7 123.5 100.9 89.4 82.6 78.0 74.7 72.0
MLAT -54.8 -61.3 67.9 -74.5 -80.9 -86.0 -83.9 -78.1 71.9 -65.7 -59.4 -53.3
MLON 323.7 324.9 326.8 330.5 338.9 18.6 97.6 117.4 123.4 126.6 129.7 130.1
MLT 20.17 20.28 20.44 20.72 21.31 24.00 5.29 6.65 7.08 7.33 7.50 7.62

FIGURE 1

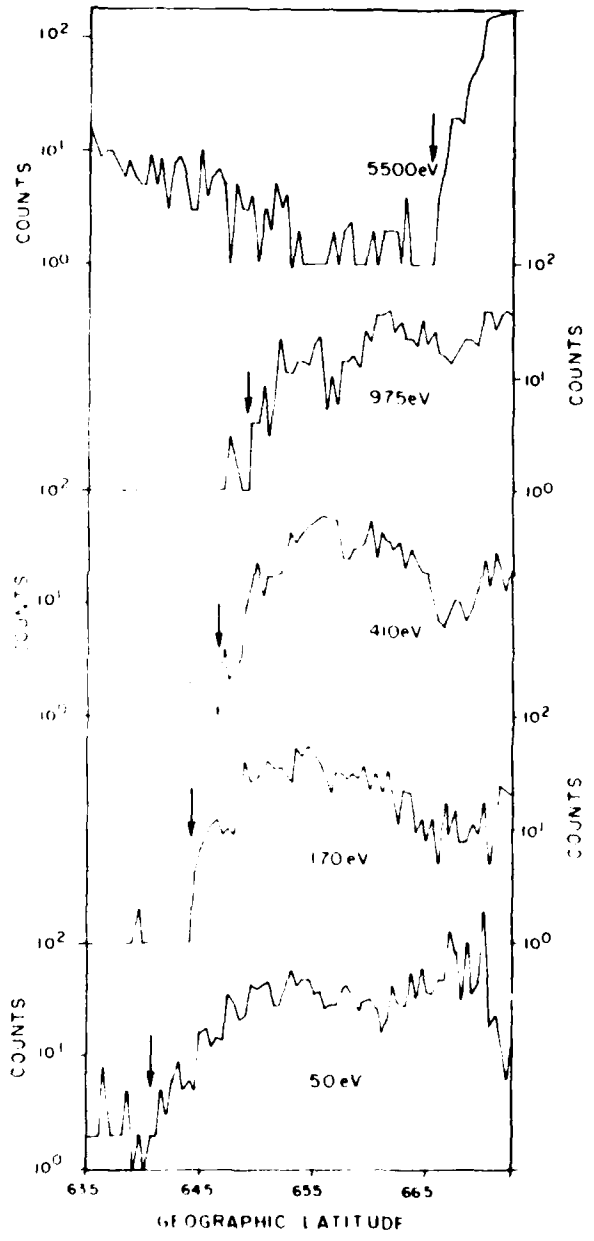
5500eV
975eV
410eV
170eV
50eV
COUNTS
GEOGRAPHIC LATITUDE
635
645
655
665

FIGURE 2

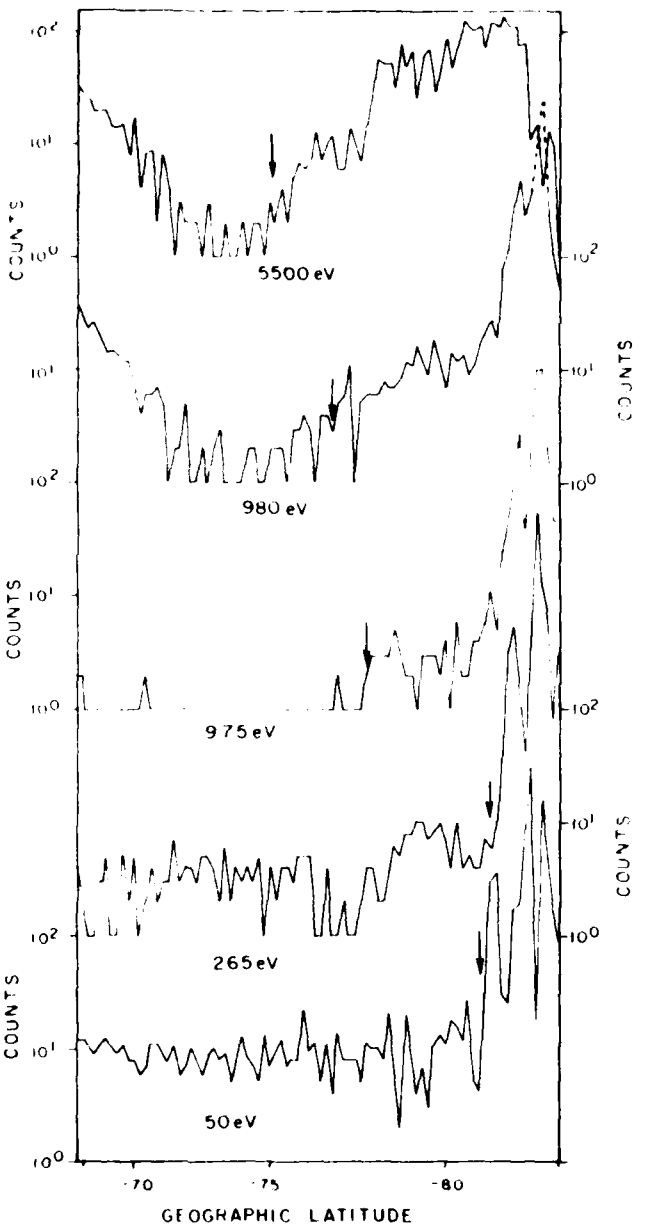
5500 eV
980 eV
975 eV
265 eV
50 eV
COUNTS
-70
-75
-80
GEOGRAPHIC LATITUDE

FIGURE 3

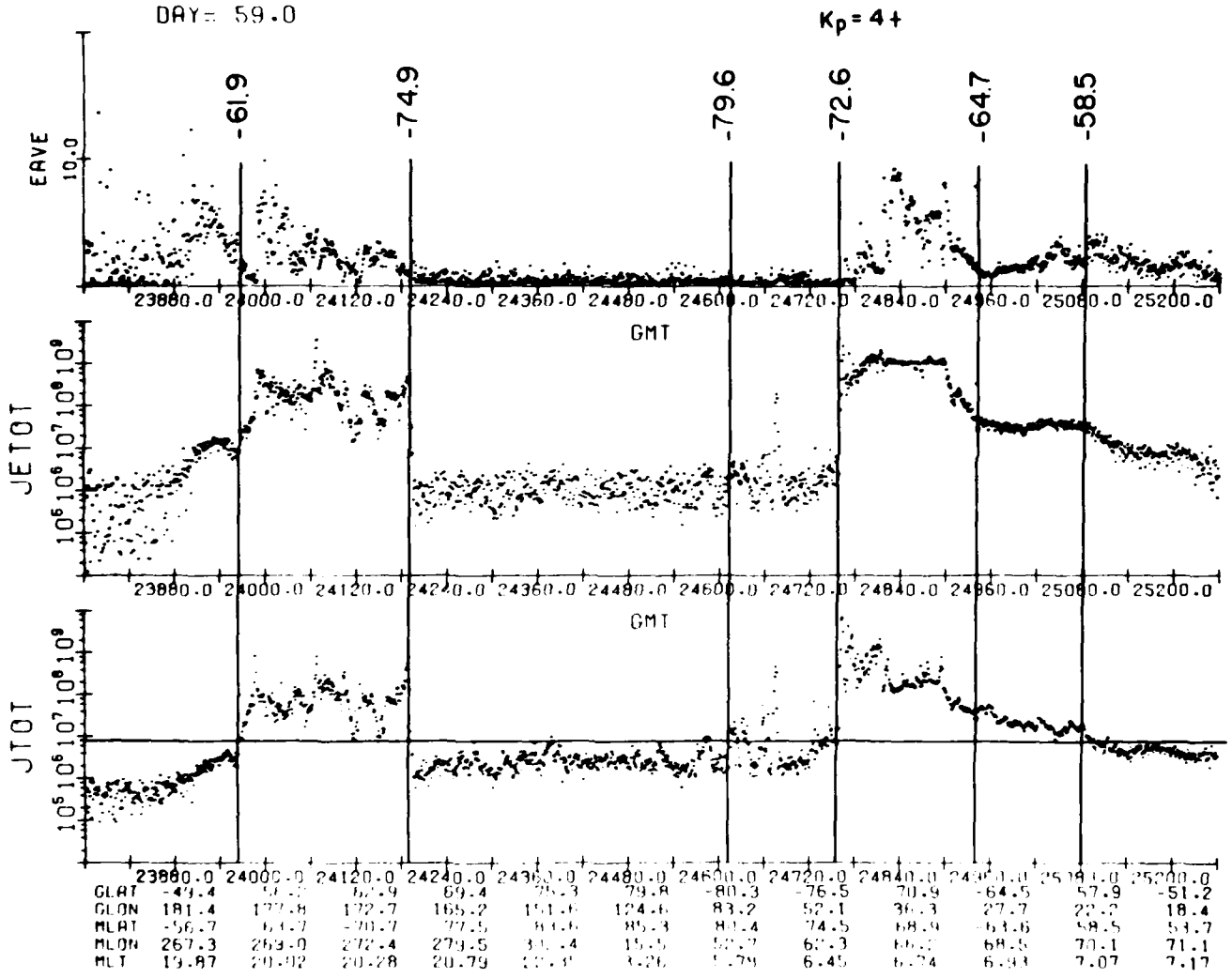
DAY= 59.0
Kp= 4+
-61.9
-74.9
-79.6
-72.6
-647
-585
EAVE
10.0
23880.0 24000.0 24120.0 24240.0 24360.0 24480.0 24600.0 24720.0 24840.0 24960.0 25080.0 25200.0
GMT
JETOT
10^6 10^7 10^8 10^9
23880.0 24000.0 24120.0 24240.0 24360.0 24480.0 24600.0 24720.0 24840.0 24960.0 25080.0 25200.0
GMT
JTOT
10^5 10^6 10^7 10^8 10^9
23880.0 24000.0 24120.0 24240.0 24360.0 24480.0 24600.0 24720.0 24840.0 24960.0 25080.0 25200.0
GLAT -49.4 -80.3 -76.5 70.9 -64.5 57.9 -51.2
GLON 181.4 122.7 165.2 124.6 83.2 52.1 27.7 18.4
MLAT -56.7 -70.7 74.5 68.9 58.5 54.7
MLON 267.3 272.4 279.5 62.3 70.1 71.1
MLT 19.87 20.28 20.79 6.45 7.07 7.17

FIGURE 4

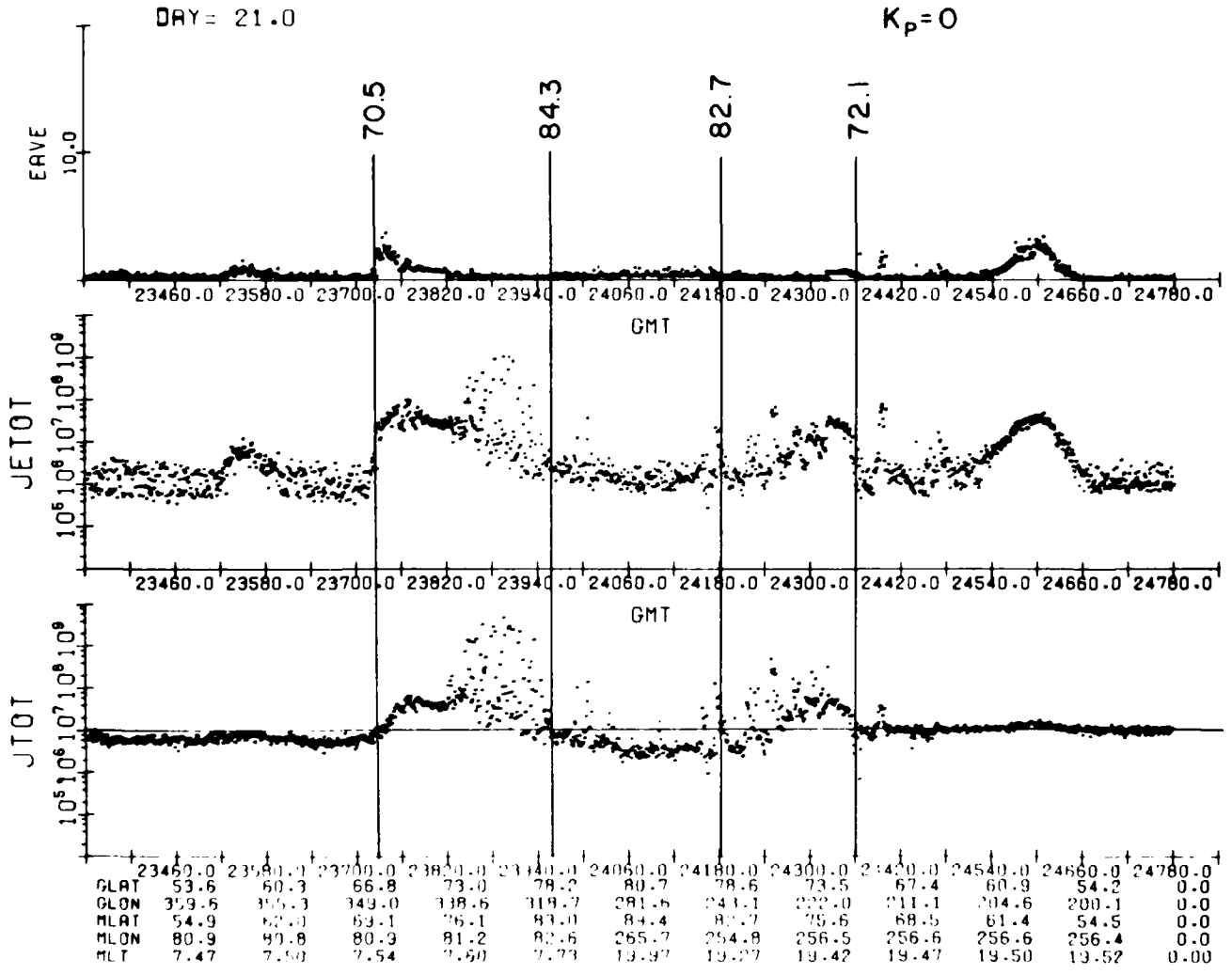
DAY= 21.0
K_p=0
70.5
84.3
82.7
72.1
EAVE
10.0
23460.0 23580.0 23700.0 23820.0 23940.0 24060.0 24180.0 24300.0 24420.0 24540.0 24660.0 24780.0
GMT
JETOT
10^5 10^6 10^7 10^8 10^9
23460.0 23580.0 23700.0 23820.0 23940.0 24060.0 24180.0 24300.0 24420.0 24540.0 24660.0 24780.0
GMT
JTOT
10^5 10^6 10^7 10^8 10^9
23460.0 23580.0 23700.0 23820.0 23940.0 24060.0 24180.0 24300.0 24420.0 24540.0 24660.0 24780.0
GLAT 53.6 60.3 66.8 73.0 78.2 80.7 78.6 73.5 67.4 60.9 54.2 0.0
GLON 359.6 355.3 349.0 338.6 319.7 281.6 241.1 222.0 211.1 204.6 200.1 0.0
MLAT 54.9 62.0 69.1 76.1 83.0 84.4 80.7 75.6 68.5 61.4 54.5 0.0
MLON 80.9 90.8 80.9 81.2 82.6 265.7 254.8 256.5 256.6 256.6 256.4 0.0
MLT 7.47 7.50 7.54 7.60 7.73 19.97 19.27 19.42 19.47 19.50 19.52 0.00

FIGURE 5

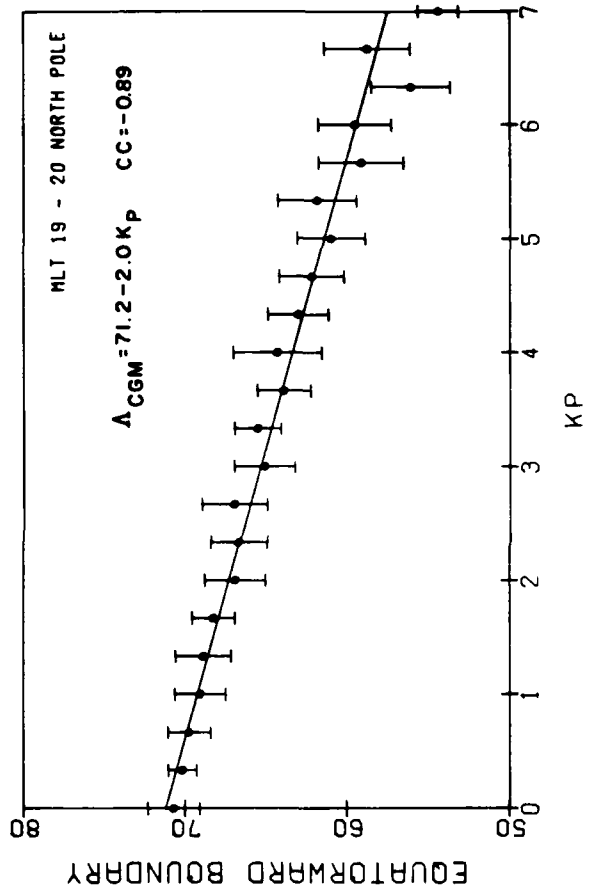
MLT 19 - 20 NORTH POLE
Λ_{CGM}=71.2-2.0 K_P CC=-0.89
EQUATORWARD BOUNDARY
80
70
60
50
0
1
2
3
4
5
6
7
KP

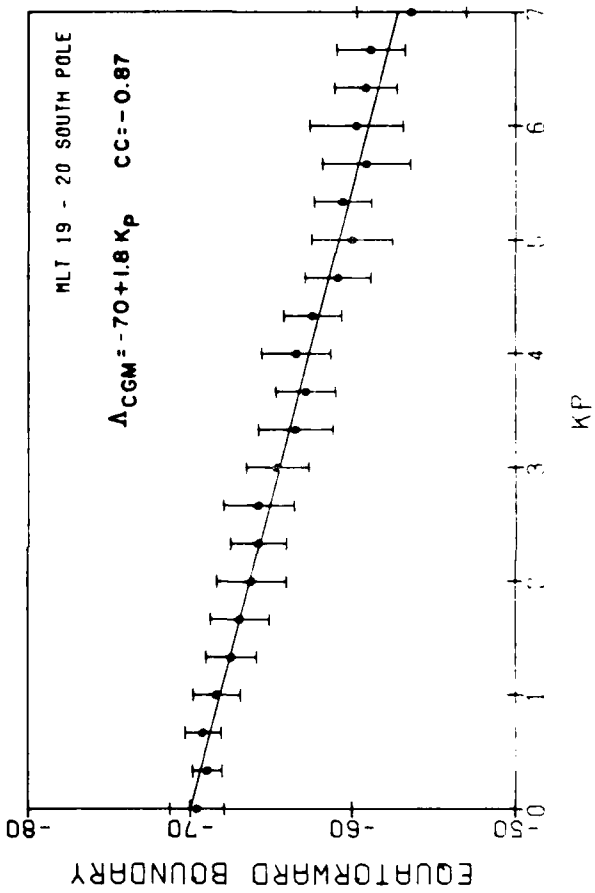
MLT 19 - 20 SOUTH POLE
Λ_{CGM}=-70+1.8 K_P CC=-0.87
EQUATORWARD BOUNDARY
-80
-70
-60
-50
0
1
4
6
7
KP

FIGURE 6

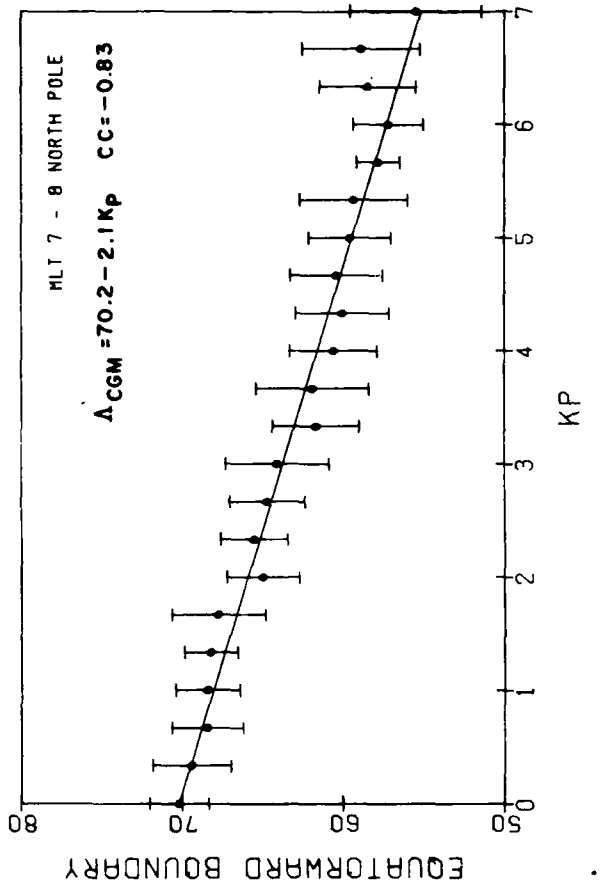
MLT 7 - 8 NORTH POLE
Λ_{CGM} =70.2−2.1K_p CC=−0.83
EQUATORWARD BOUNDARY
80
70
60
50
0
1
2
3
4
5
6
7
KP

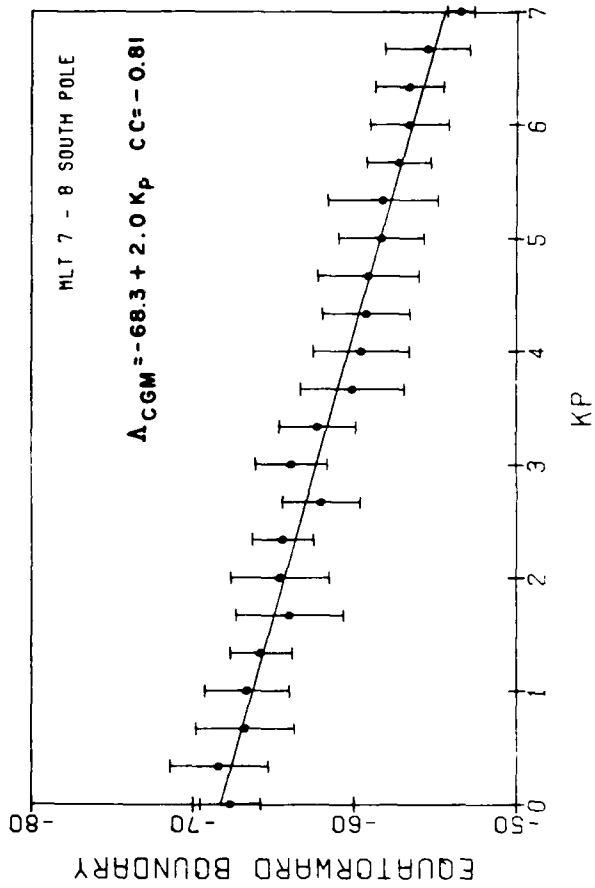
MLT 7 - 8 SOUTH POLE
Λ_{CGM} =-68.3 + 2.0 K_p CC=−0.81
EQUATORWARD BOUNDARY
-80
-70
-60
-50
0
1
2
3
4
5
6
7
KP

FIGURE 7

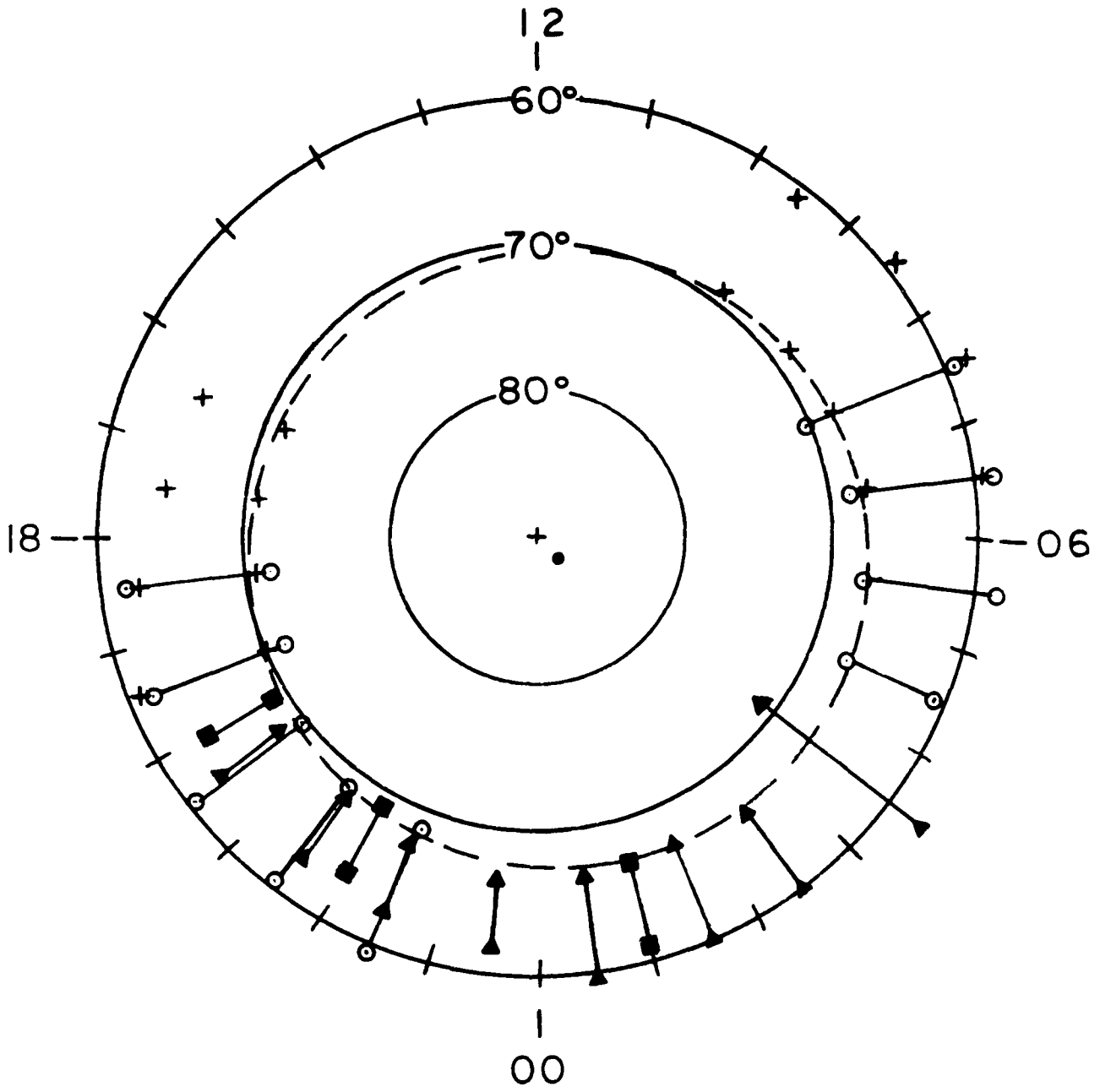

■ SHEEHAN- CAROVILLANO $K_p = 0,5$
▲ KAMIDE - WINNINGHAM $B_z = \pm 5\gamma$
⊙ NORTH POLE
\+ SOUTH POLE
} $K_p = 0,5$

FIGURE 8

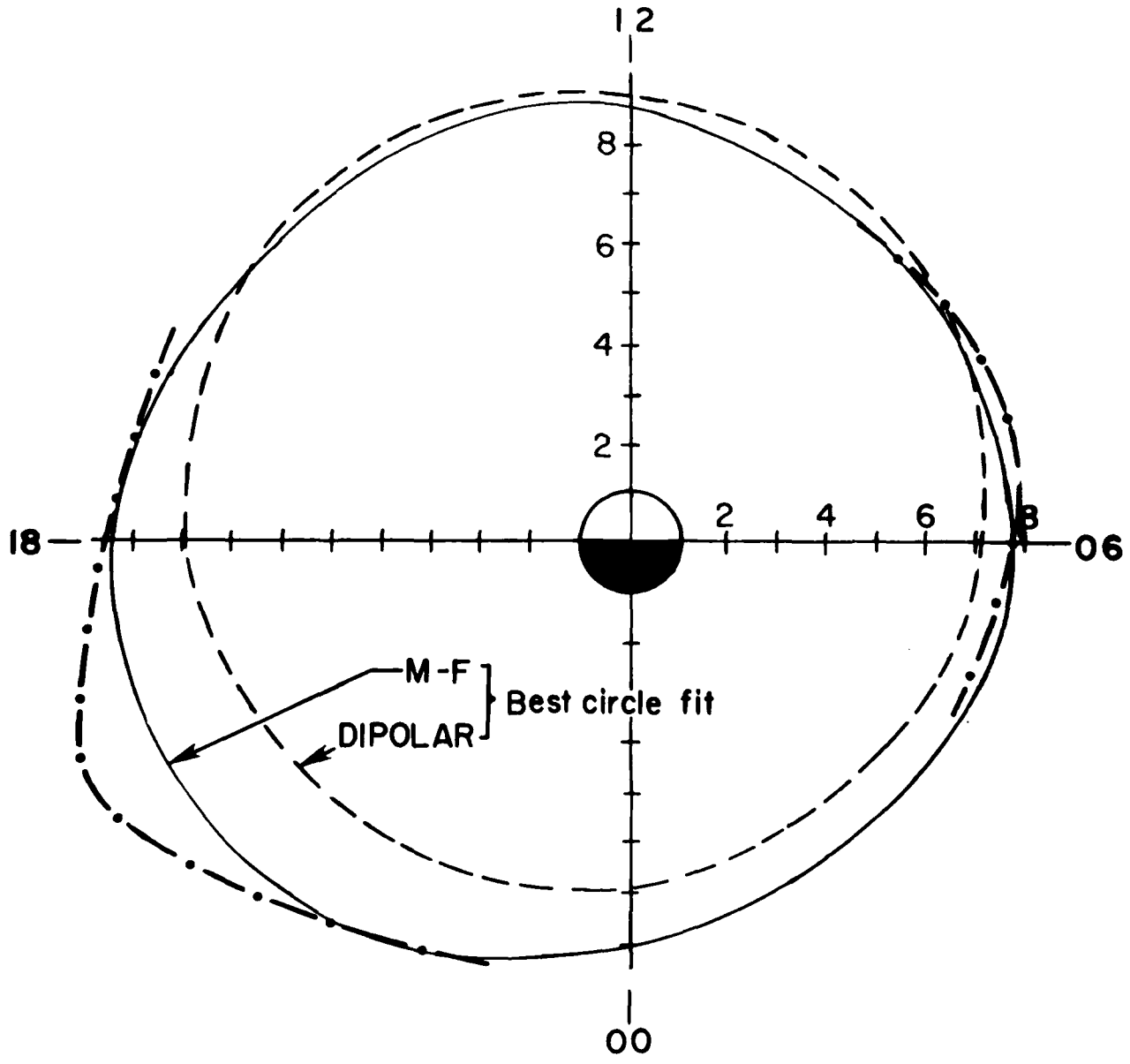

FIGURE 9

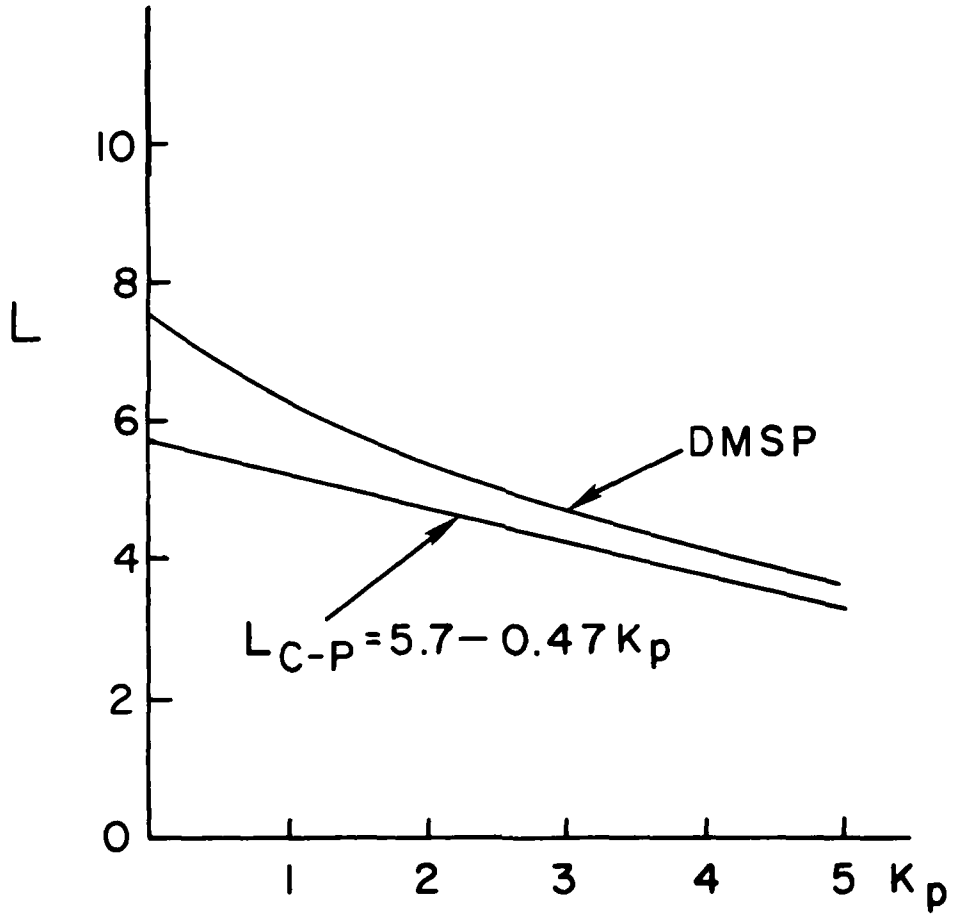

FIGURE 10

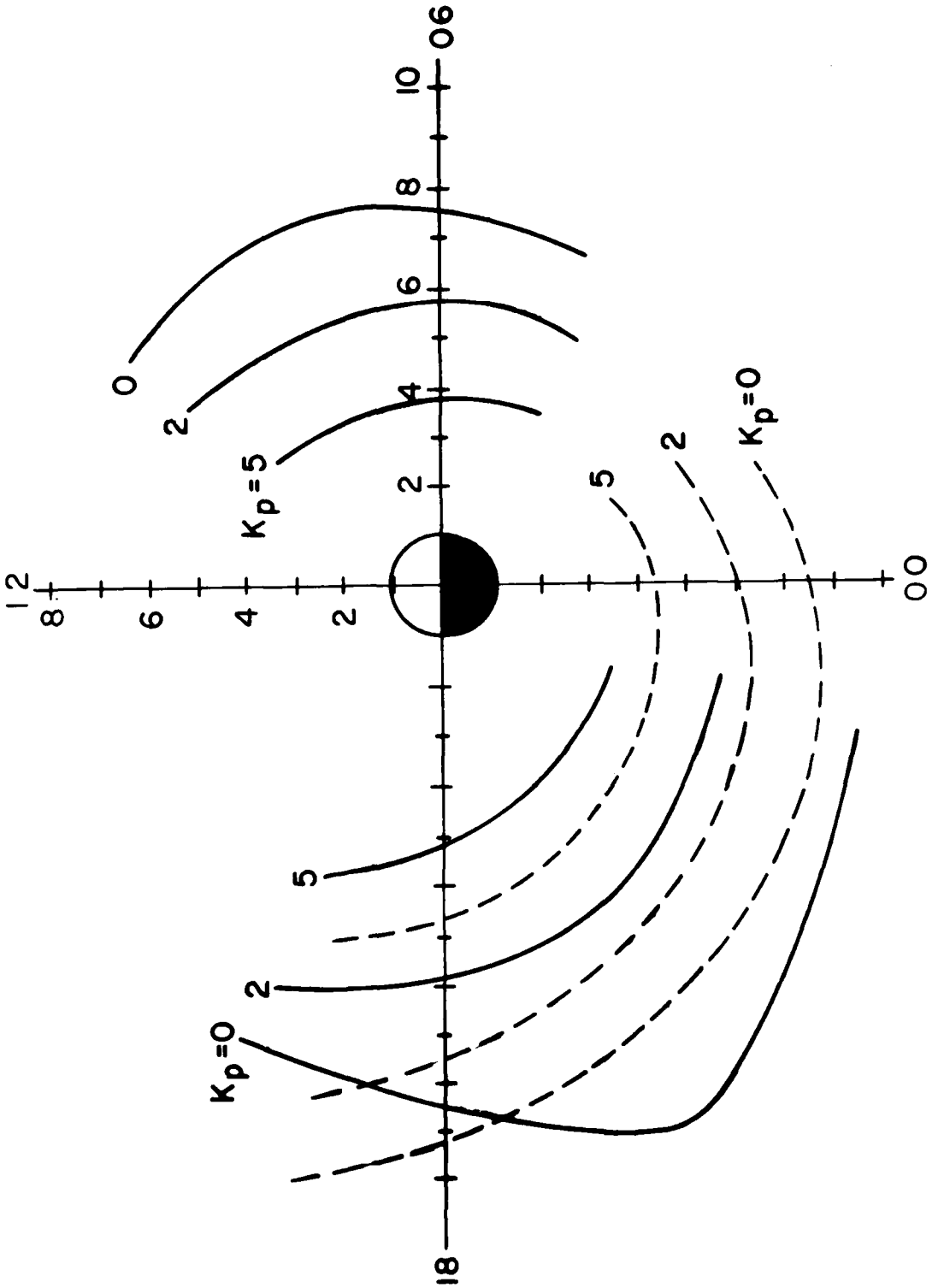

FIGURE 11

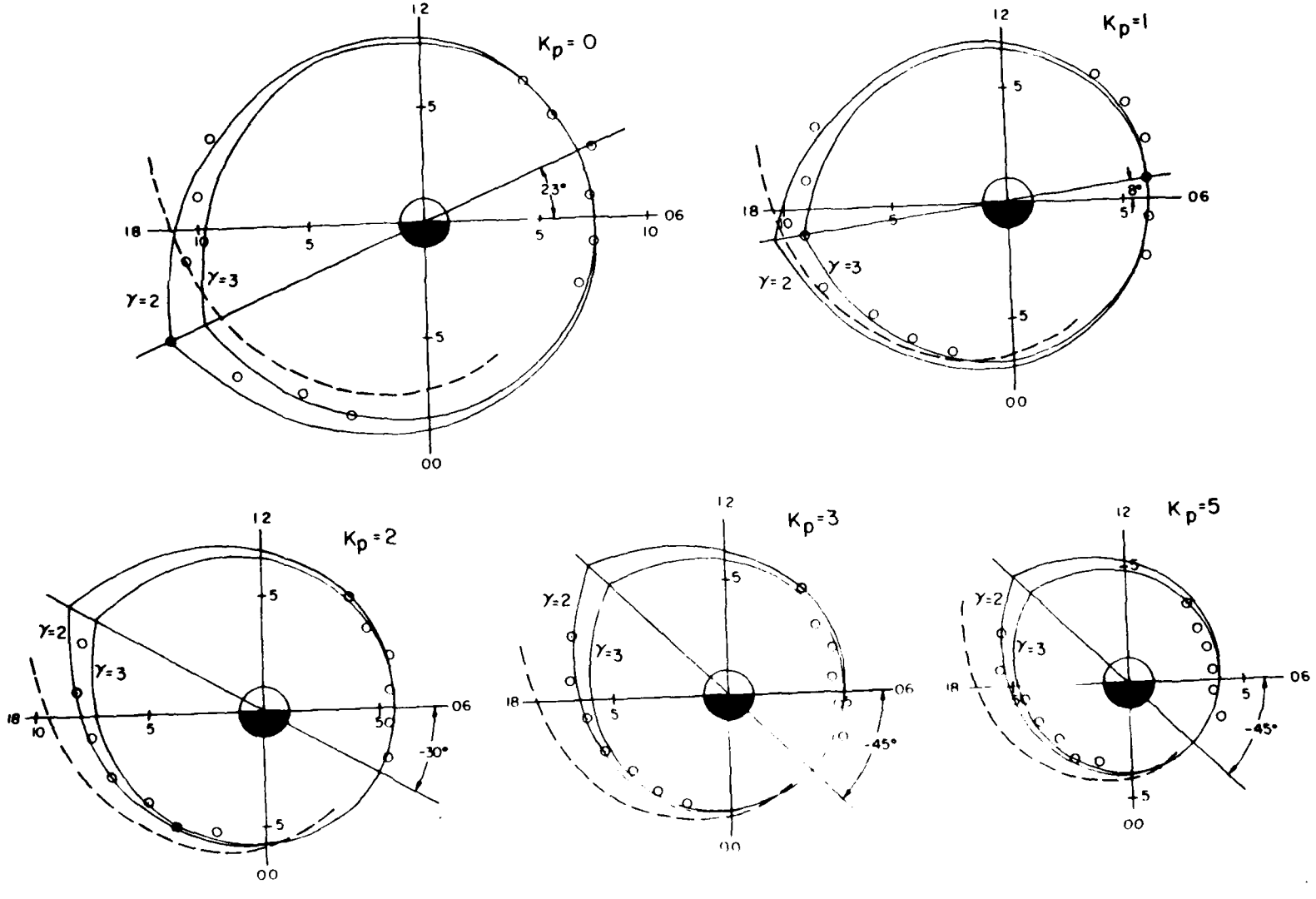
12
$K_p = 0$
5
23°
18
10
5
5
10
06
$\gamma=3$
$\gamma=2$
5
00
12
$K_p=1$
5
18
10
5
8°
5
06
$\gamma=3$
$\gamma=2$
5
00
12
$K_p=2$
5
$\gamma=2$
$\gamma=3$
18
10
5
50
06
-30°
5
00
12
$K_p=3$
5
$\gamma=2$
$\gamma=3$
18
5
06
-45°
00
12
$K_p=5$
5
$\gamma=2$
$\gamma=3$
18
5
06
-45°
5
00

FIGURE 12

COMMENTS ON "DIURNAL VARIATION OF THE AURORAL OVAL SIZE" BY CHING -I. MENG

by

M. S. Gussenhoven,[1] D. A. Hardy,[2] and W. J. Burke[1]

The position of the equatorward boundary (Λ_E) of the quiet time auroral oval has been studied by Meng (1979) using measurements from an electron spectrometer on board the DMSP (Defense Meteorological Satellite Program) satellite F2. A diurnal vairation of $\sim 4^o$ was found in the corrected geomagnetic latitudes (CGL) at which the satellite encountered this boundary. The variation was attributed to a physically unexplained 30% increase in the size of the polar cap as the north magnetic pole rotated from local midnight to local noon. Here we suggest that most of the observed variations in auroral boundaries simply reflect diurnal shifts in the satellite's trajectory in the magnetic local time - magnetic latitude (MLT-CGL) frame of reference.

The DMSP satellite is in a nearly sun-synchronous circular orbit, with an inclination of 98.8^o, centered on the 0700-1900 local time meridian. Due to the offset between the earth's spin axis and the axis of the magnetic dipole the orbit has significant diurnal variations in magnetic frames of reference. This is illustrated in Figures 1 and 2 where we have plotted the northern and southern high latitude portions of the satellite's MLT-CGL trajectories for 21 January 1978 (the quietest day in Meng's study). These trajectories are

---

1. Physics Department, Boston College, Chestnut Hill, MA 02167

2. Space Physics Division, Air Force Geophysics Laboratory, Bedford, MA 01731

representative of those followed by DMSP during the 1977-1978 winter months. At the beginning of the UT day the north polar orbit is roughly dawn to dusk crossing the noon-midnight meridian at 83° CGL in the night hemisphere. The most poleward excursions of the orbit occur between 07 and 08 UT; the most equatorward nighttime excursions are found near 1700 UT. The orbits in the southern hemisphere have the same type of motion in the opposite direction. They move from the region of the magnetic pole toward the cusp (or noon sector) often falling outside the oval entirely, and then return poleward. Since the oval lies at higher latitudes in the noon sector than in the midnight sector there are fewer possible boundary determinations to be made in the South Pole data. On the whole, the data after 12 UT on a given day is unusable for this purpose and this is reflected in the boundary data presented by Meng.

Figure 3 illustrates how diurnal variations of the DMSP orbit give rise to systematic variations in the CGL of the equatorward auroral boundary. Here we have plotted the northern hemisphere values of Λ_E detected on 21 January 1978. Meng et al. (1977) have shown that the poleward boundaries of the oval (Λ_P) during quiet times, as marked by discrete auroral arcs, are well represented by offset circles. During the period of Meng's study emissions from the oval were below the detectability levels of the DMSP optical scanner. We have assumed that during this period the oval is latitudinally narrow and that the positions of Λ_E can also be represented by offset circles. The circle in Figure 3 was chosen to fit the morning and evening values of Λ_E for the first DMSP pass of the UT day. It has a radius of 18° and is centered at 86° CGL and 0100 MLT. The circle best fitting the entire data set, in the least squares sense, has a radius of 18.5° and is centered at 86° CGL and 0115 MLT. The

corresponding southern hemisphere circle is of 19^{o} radius, centered at -87^{o} CGL and 0120 MLT. These values are consistent with quiet time averages reported by Meng et al. (1977). As seen in Figure 3 the evening oval boundary is very stable, lying along the chosen circle. The morning oval boundary is close to the plotted circle but shows much greater variability. This is consistent with results from a large set of DMSP measurements reported by Gussenhoven et al. (1979) who show that: (A) The morning equatorward boundary is much more variable than the evening boundary for a given magnetic activity. (B) For extended periods of quiet magnetic activity the oval does not become entirely stable, but can fluctuate greatly in its poleward boundaries and to a lesser extent in its equatorward boundaries.

Predicted UT modulations of Λ_E found by combining offset circles and DMSP orbital variations for the northern and southern hemispheres are given in Figures 4 and 5 respectively. The upper (lower) traces represent the afternoon-evening (morning) equatorial boundaries. Observed values of Λ_E, as determined by Meng, are plotted as triangles. Both the afternoon and morning southern hemisphere as well as the evening, northern hemisphere observations are in remarkable agreement with their predicted estimates. The morning, northern hemisphere measurements show less agreement. The overall differences would be less had we used the least squares circle as our predictor. It should also be noted that morning and evening values tracked each other better on the other days presented by Meng than they did on the first half of 21 January. Thus, on the other days the predicted and observed values of Λ_E would be in better agreement than in the case presented here.

We therefore conclude that a very large portion if not all of the diurnal auroral boundary variation reported by Meng can be explained by variations in the satellite orbit across an oval represented by an offset circle. We suggest that, in order to determine the universal time variation, either a correction for the effect of orbit change in local time could be made, or that a much greater restriction in magnetic local time be imposed.

References

Gussenhoven, M. S., D. A. Hardy, and W. J. Burke, DMSP electron observations of equatorward auroral electron boundaries and their relationship with magnetospheric electric fields, Trans. Amer. Geophys. U. 60, (in press), 1979.

Meng, Ching -I., Diurnal variation of the auroral oval size, J. Geophys. Res., 84, 5319-5324, 1979.

Meng, Ching -I., R. H. Holzworth, and S.-I. Akasofu, Auroral circle delineating the poleward boundary of the quiet auroral belt, J. Geophys. Res., 82, 164-172, 1977.

Figure Captions

Figure 1. The orbital paths of the DMSP-F2 satellite over the North pole for January 21, 1978. The orbits are plotted in corrected geomagnetic latitudes and magnetic local time. The approximate universal time for each polar crossing is given. The quiet oval is represented by an offset circle.

Figure 2. Same as Figure 1, but for South pole crossings.

Figure 3. The boundaries for the northern auroral zone as determined by Meng, plotted in corrected geomagnetic latitude and magnetic local time for January 21, 1978, along with the offset circle used to predict the diurnal variation. The small cross marks the geomagnetic pole, the large cross the center for the offset circle.

Figure 4. The solid lines show the expected dirunal variation in the equatorward boundary of the auroral zone in the northern hemisphere for both morning and evening sectors when the variation in the orbit has been taken into account and when the oval has been represented by an offset circle. The evening boundaries are shown in the upper panel (for latitude marks on the left) and the morning boundaries in the lower panel (for latitude marks on the right). The boundaries as determined by Meng are plotted as closed (evening side) and open (morning side) triangles.

Figure 5. Same as for Figure 3, but for the South pole.

SATELLITE ORBITS IN GEOMAGNETIC COORDINATES

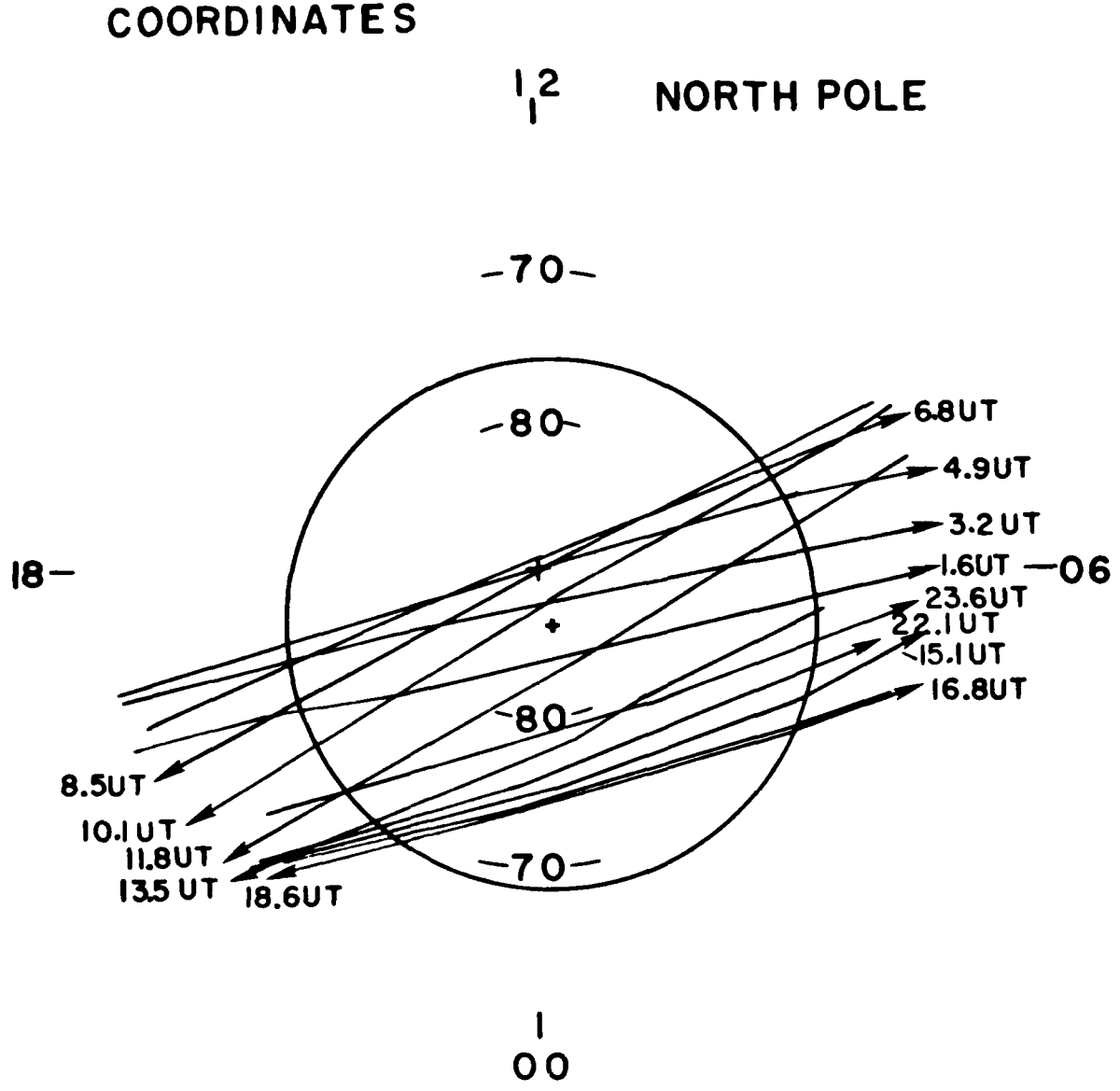

FIGURE 1

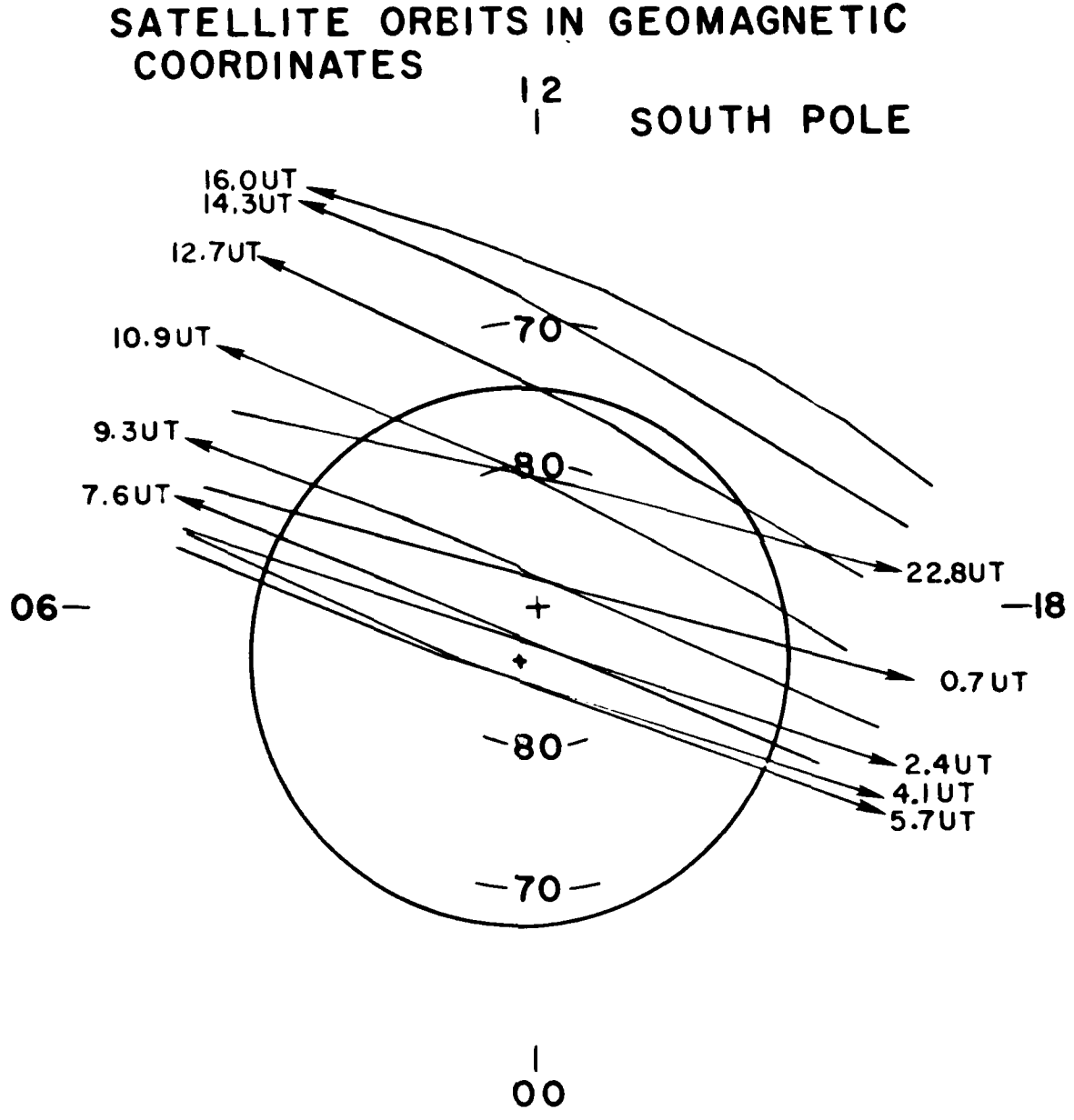
SATELLITE ORBITS IN GEOMAGNETIC COORDINATES
12
SOUTH POLE
16.0UT
14.3UT
12.7UT
10.9UT
9.3UT
7.6UT
-70-
-80-
22.8UT
06-
-18
0.7UT
-80-
2.4UT
4.1UT
5.7UT
-70-
00

FIGURE 2

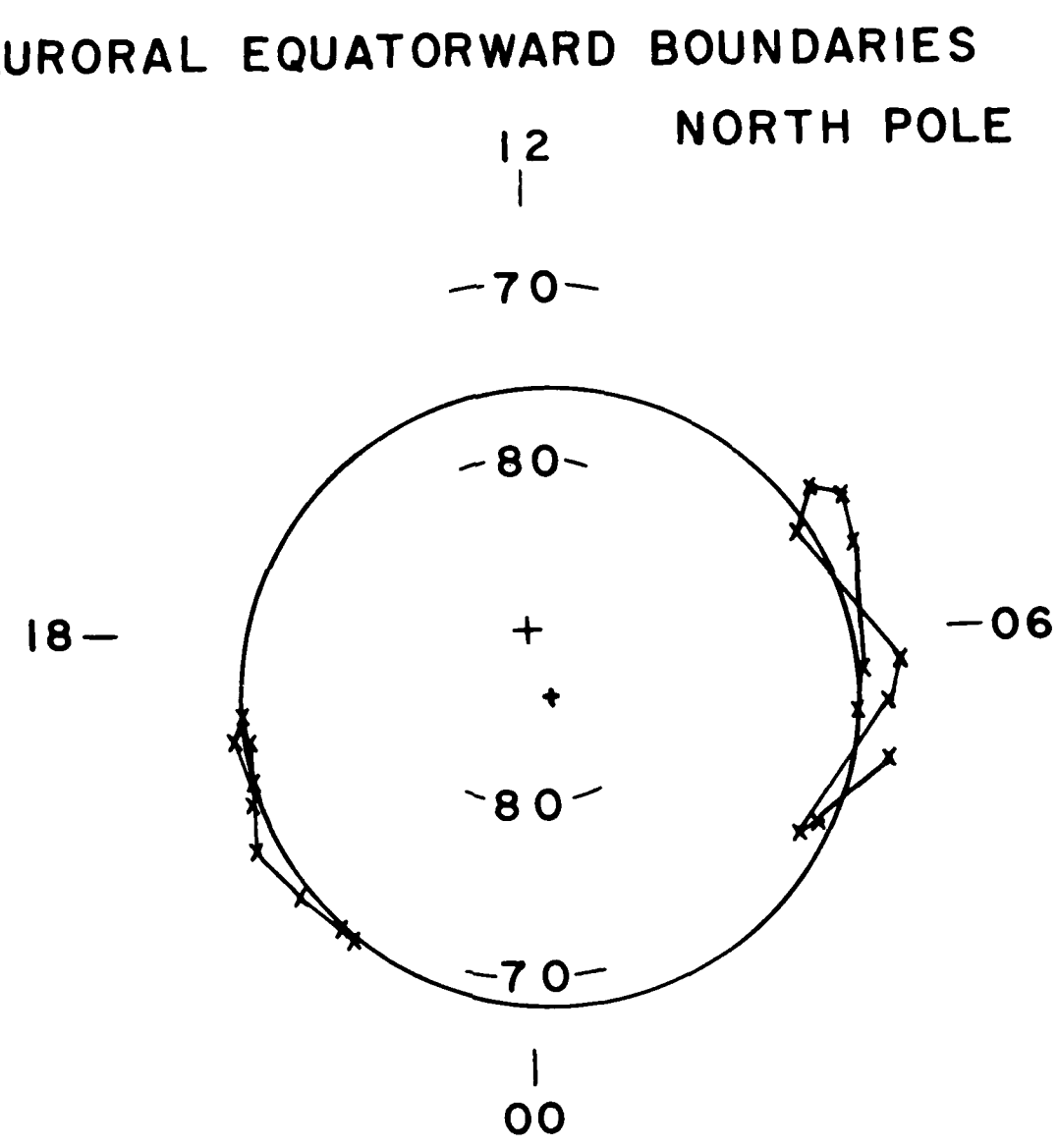
AURORAL EQUATORWARD BOUNDARIES
NORTH POLE
12
-70-
-80-
18-
-06
-80-
-70-
00

FIGURE 3

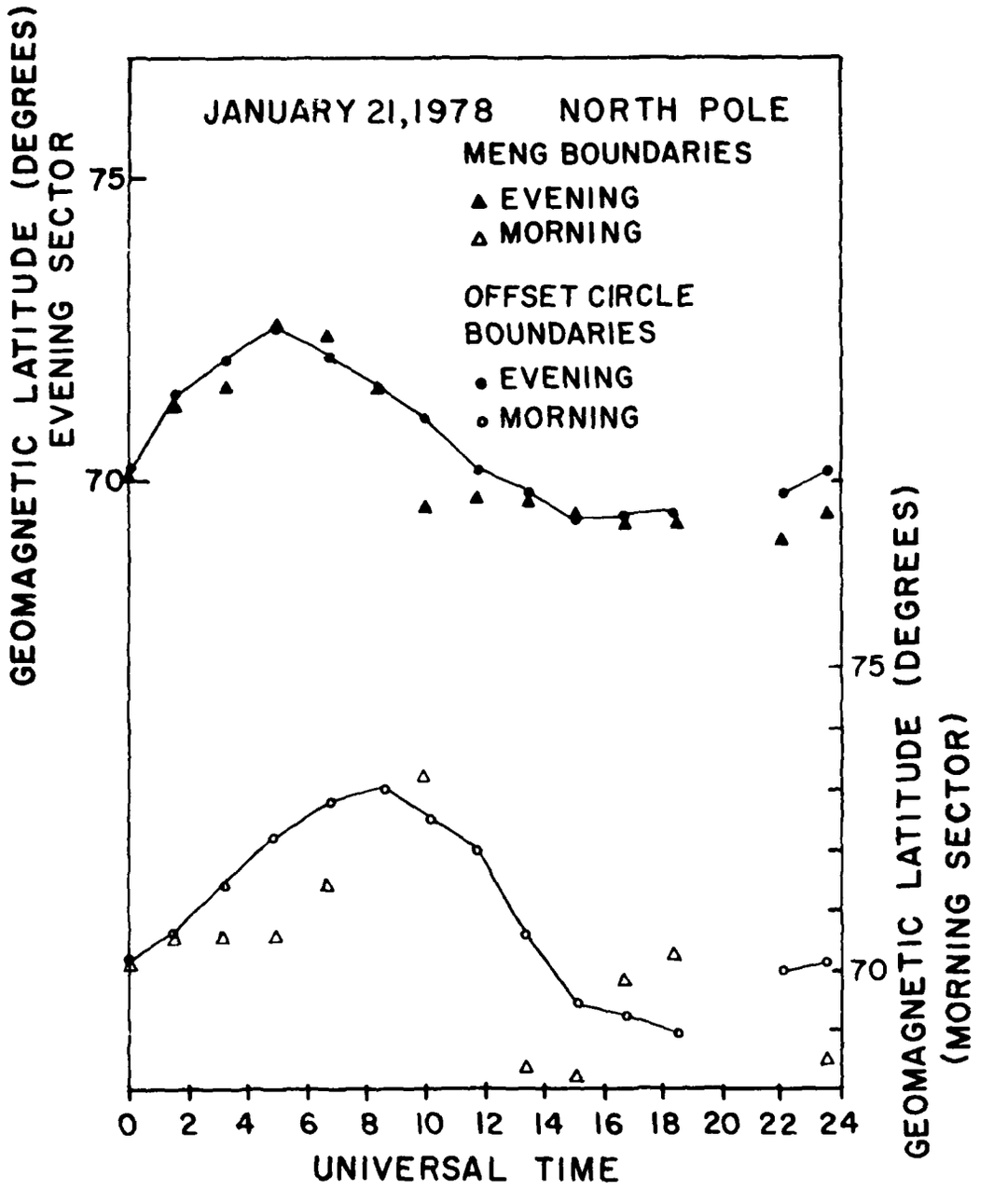
JANUARY 21, 1978 NORTH POLE
MENG BOUNDARIES
▲ EVENING
△ MORNING
OFFSET CIRCLE BOUNDARIES
● EVENING
○ MORNING
GEOMAGNETIC LATITUDE (DEGREES) EVENING SECTOR
75
70
GEOMAGNETIC LATITUDE (DEGREES) (MORNING SECTOR)
75
70
0 2 4 6 8 10 12 14 16 18 20 22 24
UNIVERSAL TIME

FIGURE 4

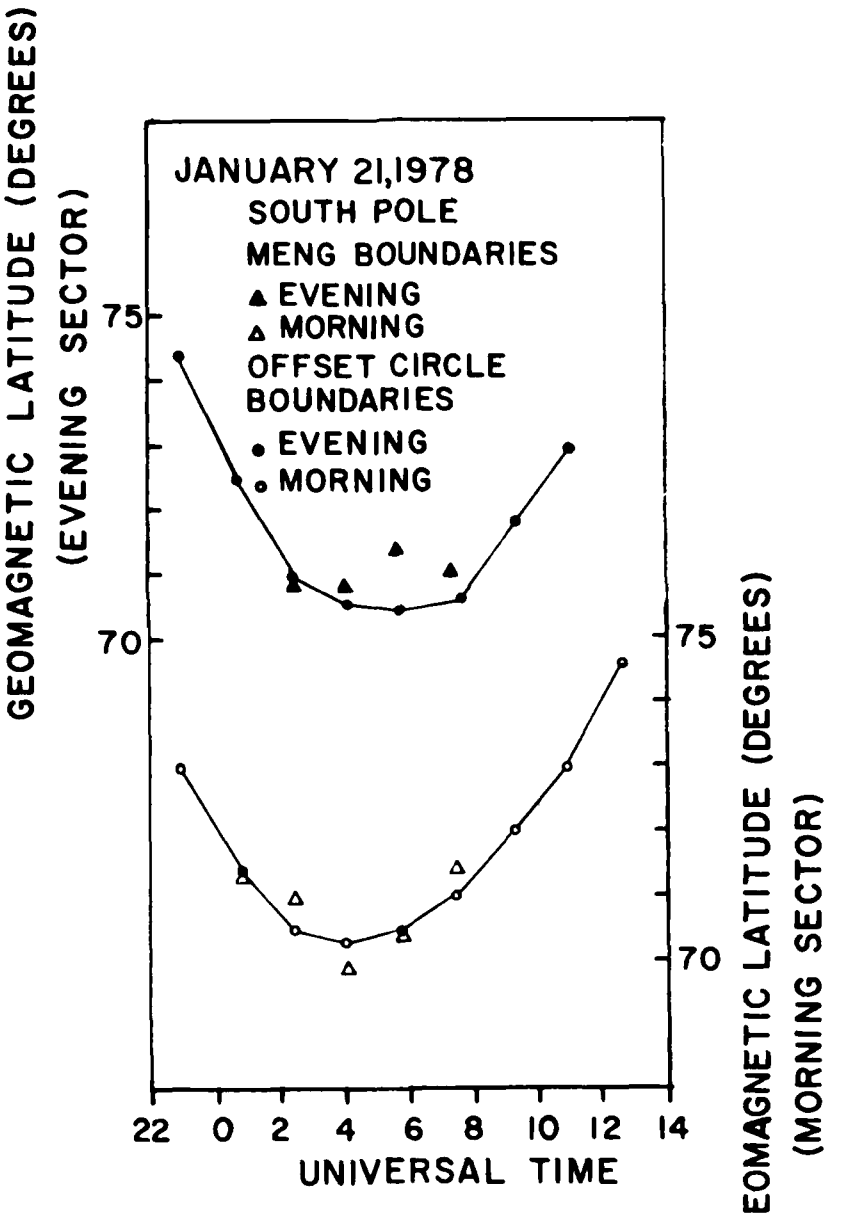
JANUARY 21,1978
SOUTH POLE
MENG BOUNDARIES
▲ EVENING
△ MORNING
OFFSET CIRCLE
BOUNDARIES
● EVENING
○ MORNING
GEOMAGNETIC LATITUDE (DEGREES)
(EVENING SECTOR)
75
70
22 0 2 4 6 8 10 12 14
UNIVERSAL TIME
75
70
GEOMAGNETIC LATITUDE (DEGREES)
(MORNING SECTOR)

FIGURE 5